

ASTRONOMICAL INSTITUTE
SLOVAK ACADEMY OF SCIENCES

CONTRIBUTIONS
OF THE ASTRONOMICAL OBSERVATORY
SKALNATÉ PLESO

• VOLUME L •

Number 3



July 2020

Editorial Board

Editor-in-Chief

Augustín Skopal, *Tatranská Lomnica, The Slovak Republic*

Managing Editor

Richard Komžík, *Tatranská Lomnica, The Slovak Republic*

Editors

Drahomír Chochol, *Tatranská Lomnica, The Slovak Republic*

Július Koza, *Tatranská Lomnica, The Slovak Republic*

Aleš Kučera, *Tatranská Lomnica, The Slovak Republic*

Luboš Neslušan, *Tatranská Lomnica, The Slovak Republic*

Vladimír Porubčan, *Bratislava, The Slovak Republic*

Theodor Pribulla, *Tatranská Lomnica, The Slovak Republic*

Advisory Board

Bernhard Fleck, *Greenbelt, USA*

Arnold Hanslmeier, *Graz, Austria*

Marian Karlický, *Ondřejov, The Czech Republic*

Tanya Ryabchikova, *Moscow, Russia*

Giovanni B. Valsecchi, *Rome, Italy*

Jan Vondrák, *Prague, The Czech Republic*



Astronomical Institute of the Slovak Academy of Sciences
2020

ISSN: 1336–0337 (on-line version)

CODEN: CAOPF8

Editorial Office: Astronomical Institute of the Slovak Academy of Sciences
SK - 059 60 Tatranská Lomnica, The Slovak Republic

CONTENTS

EDITORIAL

A. Skopal, R. Komžík: Editorial	647
--	-----

STARS

T. Pribulla, L. Hambálek, E. Guenther, R. Komžík, E. Kundra, J. Nedoroščík, V. Perdelwitz, M. Vaňko: Close eclipsing binary BD And: a triple system	649
V. Andreoli, U. Munari: LAMOST J202629.80+423652.0 is not a symbiotic star	672
M. Yu. Skulsky: Formation of magnetized spatial structures in the Beta Lyrae system. I. Observation as a research background of this phenomenon	681
R. Hudec, E. Splittgerber: Note on magnitude estimation on digi- tized astronomical photographic plates	704

The Contributions of the Astronomical Observatory Skalnaté Pleso
are available in a full version
in the frame of ADS Abstract Service
and can be downloaded in a usual way from the URL address:

<https://ui.adsabs.harvard.edu/>

as well as from the web-site of
the Astronomical Institute of the Slovak Academy of Sciences
on the URL address:

<https://www.astro.sk/caosp/caosp.php>

The journal is covered/indexed by:

Thomson Reuters services (ISI)

Science Citation Index Expanded (also known as SciSearch®)
Journal Citation Reports/Science Edition

SCOPUS

EDITORIAL

During 2019, the journal Contributions of the Astronomical Observatory Skalnaté Pleso (CAOSP) published 81 papers on 562 pages within three issues. The journal received 145 citations and increased its impact factor to 0.833 for 2018 - the highest value to date.

Volume 49/1 presents two regular papers, one containing a large contribution on the recent photometry of symbiotic stars - XIV. part, which continues our long-lasting monitoring program of these objects, we started in 1991.

Volume 49/2 contains contributions based on lectures from proceedings of the workshop "Observing techniques, instrumentation and science for metre-class telescopes II", held in Tatranská Lomnica during September 24-28, 2018.

Other regular articles were published in Volume 49/3 together with seven contributions based on lectures from the joint ERASMUS+ and OPTICON summer schools held in Stará Lesná between 17 and 27 July, 2019.

During 2020 we plan to publish two special issues from international conferences and at least one issue containing regular articles. The first special issue is scheduled for Volume 50/1 and represents proceedings from "12th Serbian Conference on spectral line shapes in astrophysics", held in Vrdnik, Serbia, June 3-7, 2019, and the second one is allocated for proceedings from the conference, "Universe of Binaries, Binaries in the Universe", held in Telč, Czech republic, September 7 - 11, 2019.

Finally, during 2019 we established assignment of the digital object identifier (DOI) to each article published by CAOSP, being in effect from January 1, 2020.

Tatranská Lomnica, January 7, 2020

Augustín Skopal, Editor-in-Chief

Richard Komžík, Managing Editor

Close eclipsing binary BD And: a triple system

T. Pribulla^{1,2,3}, L. Hambálek¹, E. Guenther⁴, R. Komžík¹,
E. Kundra¹, J. Nedoroščík⁴, V. Perdelwitz⁵ and M. Vaňko¹

¹ *Astronomical Institute of the Slovak Academy of Sciences
059 60 Tatranská Lomnica, The Slovak Republic, (E-mail: pribulla@ta3.sk)*

² *ELTE, Gothard Astrophysical Observatory, 9700 Szombathely,
Szent Imre h. u. 112, Hungary*

³ *MTA-ELTE Exoplanet Research Group, 9700 Szombathely,
Szent Imre h. u. 112, Hungary*

⁴ *Thüringer Landessternwarte, Sternwarte 5, 077 78 Tautenburg, Germany*

⁵ *Hamburger Sternwarte, Gojenbergsweg 112, 21029 Hamburg, Germany*

Received: October 21, 2019; Accepted: January 8, 2020

Abstract. BD And is a fairly bright ($V = 10.8$), active and close ($P \sim 0.9258$ days) eclipsing binary. The cyclic variability of the apparent orbital period as well as third light in the light curves indicate the presence of an additional late-type component. The principal aim is the spectroscopic testing of the third-body hypothesis and determination of absolute stellar parameters for both components of the eclipsing binary. First medium and high-resolution spectroscopy of the system was obtained. The broadening-function technique appropriate for heavily-broadened spectra of close binaries was used. The radial velocities were determined fitting the Gaussian functions and rotational profiles to the broadening functions. A limited amount of photometric data has also been obtained. Although the photometric observations were focused on the obtaining the timing information, a cursory light-curve analysis was also performed. Extracted broadening functions clearly show the presence of a third, slowly-rotating component. Its radial velocity is within error of the systemic velocity of the eclipsing pair, strongly supporting the physical bond. The observed systemic radial-velocity and third-component changes do not support the 9 year orbit found from the timing variability. Masses of the components of the eclipsing pair are determined with about 0.5% precision. Further characterization of the system would require long-term photometric and spectroscopic monitoring.

Key words: Stars: individual: BD And; Stars: binaries: eclipsing; Methods: observational; Techniques: spectroscopy

1. Introduction

Gravitational perturbations of a primordial wide binary by a third body cause so called Kozai-Lidov cycles (Kozai, 1962). Cyclic variations of eccentricity of the inner binary and changes of the mutual inclination can occur if the mutual

inclination, j , of the inner and outer orbital planes is $39^\circ < j < 141^\circ$. During the resulting close approaches of the inner binary components in the eccentric orbit tidal friction reduces orbital energy, bringing them closer. If this process is the only evolutionary channel to produce close binary stars, all close binaries must be accompanied by a third body. Unfortunately, the observational evidence is strongly biased by techniques used to detect often faint third components. While Pribulla & Rucinski (2006), who used several techniques and numerous observations, found at least 2/3 of contact binaries to reside in triple or multiple systems, Rappaport et al. (2013), who searched for eclipse timing variations (light-time effect, LiTE) in the *Kepler* data, found only about 20% of eclipsing binaries to be members of triple systems.

The eclipse-timing technique is sensitive to third components on long-period orbits (see e.g. Pribulla et al., 2012) but it gives only an indication because other effects can produce similar variability, e.g. mass transfer or magnetic-orbital momentum coupling (Applegate, 1992). Much more conclusive is the spectroscopic (Pribulla et al., 2006) or visual (Tokovinin et al., 2010) detection. There is, however, still some low probability that the additional component is physically unrelated. In the case of a wide third-body orbit, the systemic radial velocity (RV) of the binary should be close to the RV of the third component. For tighter systems mutual orbital revolution is the ultimate proof (Pribulla et al., 2008). An analysis of eclipses in triple systems can sometimes lead not only to confirmation of multiplicity, but to accurate determination of orbital and component parameters (see e.g. Carter et al., 2011).

BD And (GSC 3635-1320) is a close ($P \sim 0.9258$ days), and relatively bright ($V_{\max} = 10.8$) eclipsing binary. It was discovered by Parenago (1938) and subsequently analyzed by Florja (1938), who classified BD And as an Algol-type eclipsing binary with orbital period 0.462899 days and 0.46 and 0.09 mag deep minima. BD And was identified as a ROSAT source by Shaw et al. (1996), and it was detected by Swift (Evans et al., 2013) and twice in the course of the XMM-Newton Slew Survey (XMM-SSC, 2018), indicating that the source has a high level of magnetic activity. Only recently, Sipahi & Dal (2014) obtained CCD *BVR* photometry of the system and found that (i) the true orbital period is two times longer than determined previously, (ii) the mass ratio of the eclipsing binary is about 0.97, (iii) minima times show a cyclic variability indicating presence of a third body on about 9.6-year orbit, and (iv) light variation outside the primary eclipse may result from γ Dor oscillations of the primary component. Subsequently Kim et al. (2014) analyzed extensive new *BVR* photometry as well as published timing data. The data analysis confirmed periodic orbital period variations indicating a third component revolving on a highly eccentric orbit with $e \sim 0.76$. The light-curve (LC) variability was interpreted by dark photospheric spots on the hotter component. An LC analysis showed about 14% third-light contribution. None of the above observations showed any flares in spite of the strong spot activity indicated by a large and variable LC asymmetry.

Unfortunately, no spectroscopic observations have been published yet, leaving the question of the system's multiplicity open. Therefore, we observed BD And spectroscopically from 2016 to 2019 and obtained additional BVI_c CCD photometry.

The layout of the paper is as follows. In Section 2, we briefly describe new spectroscopic and photometric observations. In Section 3, we present the analysis of the spectroscopy. The timing variability is presented in Section 4 while LC and broadening-function (hereafter BF) modeling in Section 5. Third-body parameters and orbit are discussed in Section 6. The surface activity of the close binary in Section 7. The paper is concluded in Section 8.

2. New observations and data reduction

2.1. Échelle spectroscopy

Medium and high-dispersion spectroscopy of BD And was obtained with three spectrographs. At Stará Lesná observatory the observations were performed at the G1 pavilion with a 60cm, f/12.5 Zeiss Cassegrain telescope equipped with a fiber-fed échelle spectrograph eShel (see Thizy & Cochar, 2011; Pribulla et al., 2015). The spectrograph has a 4150-7600 Å (24 échelle orders), spectral range and a maximum resolving power of about $R = 11,000$. The ThAr calibration unit provides about 100 m s^{-1} RV accuracy. An Atik 460EX CCD camera, which has a 2749×2199 array chip, $4.54 \mu\text{m}$ square pixels, read-out noise of 5.1 e^- and gain $0.26 \text{ e}^-/\text{ADU}$, was used as the detector. The observations were also performed with a 1.3m, f/8.36, Nasmyth-Cassegrain telescope equipped with a fiber-fed échelle spectrograph at Skalnaté Pleso. Its layout follows the MUSICOS design (see Baudrand & Bohm, 1992). The spectra were recorded by an Andor iKon-L DZ936N-BV CCD camera, with a 2048×2048 array, $13.5 \mu\text{m}$ square pixels, 2.9 e^- read-out noise and gain close to unity. The spectral range of the instrument is 4250-7375 Å (56 échelle orders) with the maximum resolution of $R = 38,000$. Additional spectra were obtained at Thüringer Landessternwarte Tautenburg with the Alfred Jensch 2m telescope and coudé échelle spectrograph. These spectra cover 4510-7610 Å in 51 orders. A $2.2''$ slit was used for all observations giving $R = 31,500$. The journal of observations is in Appendix A.

Because of the short orbital period of BD And of $P \sim 0.9258$ days, the exposure times were limited to 900 seconds (about 1.1% of the orbital period) to prevent orbital-motion smearing.

The raw data obtained with the 60cm and 1.3m telescopes were reduced using IRAF package tasks, Linux shell scripts and FORTRAN programs as described in Pribulla et al. (2015). In the first step, master dark frames were produced. In the second step, the photometric calibration of the frames was done using dark and flat-field frames. Bad pixels were cleaned using a bad-pixel mask, cosmic hits were removed using the program of Pych (2004). Order positions were defined by fitting Chebyshev polynomials to tungsten-lamp and blue LED spec-

Table 1. Journal of photometric observations of BD And. The table lists evening date (yyyymmdd), orbital phase range, No. of points, photometric filter, estimated scatter, time of the minimum light, and the instrument used. The instruments are: G1 - SBIG CCD camera in G1 pavilion at Stará Lesná and G2 - FLI CCD camera in G2 pavilion at Stará Lesná. The phases were computed using the same ephemeris as in Table 5.

Date	Phases	No.	Filter	σ	HJD _{min} 2 400 000+	Inst.
20170809	0.890 - 1.000	217	<i>B</i>	0.0034	–	G2
20170809	0.890 - 1.000	214	<i>I</i>	0.0033	–	G2
20170810	0.025 - 0.081	111	<i>B</i>	0.0042	–	G2
20170810	0.023 - 0.081	116	<i>I</i>	0.0046	–	G2
20170815	0.171 - 0.484	560	<i>B</i>	0.0029	–	G2
20170815	0.171 - 0.484	524	<i>I</i>	0.0031	–	G2
20171107	0.758 - 1.130	502	<i>B</i>	0.0032	58065.40493(13)	G2
20171107	0.757 - 1.131	504	<i>V</i>	0.0040	58065.40581(8)	G2
20171115	0.494 - 0.604	134	<i>V</i>	0.0038	–	G1
20171116	0.537 - 0.548	14	<i>V</i>	0.0049	–	G1
20171124	0.139 - 0.214	88	<i>V</i>	0.0045	–	G1
20180720	0.454 - 0.580	208	<i>B</i>	0.0036	58320.46604(4)	G2
20180720	0.455 - 0.580	204	<i>I</i>	0.0044	58320.46593(8)	G2
20180724	0.752 - 0.951	314	<i>B</i>	0.0031	–	G2
20180724	0.752 - 0.951	307	<i>I</i>	0.0038	–	G2
20180803	0.471 - 0.767	471	<i>B</i>	0.0027	58334.35305(6)	G2
20180803	0.471 - 0.768	471	<i>I</i>	0.0032	58334.35279(16)	G2
20180804	0.547 - 0.621	117	<i>B</i>	0.0030	–	G2
20180804	0.548 - 0.620	116	<i>I</i>	0.0037	–	G2
20180807	0.841 - 0.094	394	<i>B</i>	0.0029	58338.51898(4)	G2
20180807	0.842 - 0.094	397	<i>I</i>	0.0032	58338.51901(4)	G2
20180909	0.000 - 0.000	226	<i>B</i>	0.0027	58371.38370(6)	G2
20180909	0.000 - 0.000	219	<i>I</i>	0.0036	58371.38393(4)	G2
20180921	0.000 - 0.000	317	<i>B</i>	0.0025	58383.41891(13)	G2
20180921	0.000 - 0.000	299	<i>I</i>	0.0035	58383.41915(10)	G2
20181123	0.000 - 0.000	350	<i>B</i>	0.0026	58446.37438(6)	G2
20181123	0.000 - 0.000	353	<i>I</i>	0.0034	58446.37445(7)	G2

tra. In the following step, scattered light was modeled and subtracted. Aperture spectra were then extracted for both the object and the ThAr lamp and then the resulting 2D spectra were dispersion solved. The spectra obtained at TLS were reduced under the IRAF environment (see Hatzes et al., 2005; Guenther et al., 2009; Hartmann et al., 2010).

2.2. CCD photometry

A limited amount of *BVI* photometric data was obtained. Its primary goal was to better define the ephemeris for the spectroscopic observations. The data were obtained at the Stará Lesná observatory with a 18cm f/10 auxiliary Maksutov-Cassegrain telescope attached to the Zeiss 60cm Cassegrain used to obtain the échelle spectroscopy (G1 pavilion). An SBIG ST10 XME CCD camera and the Johnson-Cousins filters were used. The field of view (FoV) of the CCD camera

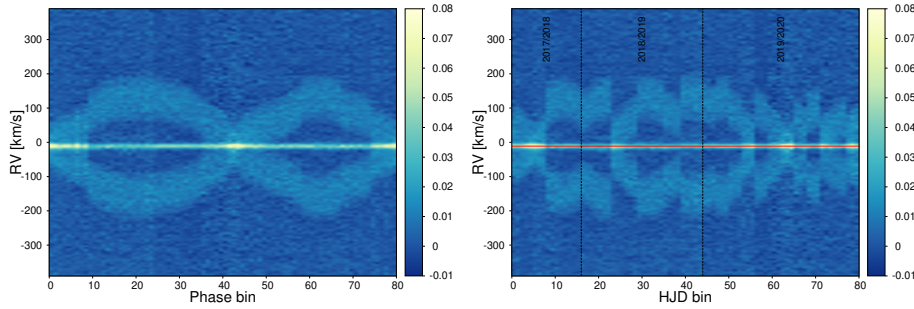


Figure 1. Broadening functions of BD And extracted from the MUSICOS spectra sorted in phase (left) and ordered by date (right). The red horizontal line denotes the average radial velocity of the third component. The vertical dashed black lines separate individual observing seasons.

is $28.5 \times 18.9'$. Additional photometry was obtained with another 60cm Zeiss Cassegrain telescope (G2 pavilion) using a Fingerlakes ML 3041 with a back-illuminated CCD (FoV is $14.1 \times 14.1'$). The filter set is also close to the Johnson-Cousins system.

The CCD frames were photometrically reduced under the IRAF environment. First, master dark and flat-field frames were produced, then bad pixels were cleaned and the frames were photometrically calibrated. Prior to aperture photometry all frames were astrometrically solved to define the pixel to WCS¹ transformation. To minimize the effects of the second-order extinction, 7 nearby stars (No. 9, 11, 12, 15, 16, 19, and 20 following designation in Table 1 of Kim et al., 2014) with the total effective color ($B - V$) = 0.586, close to that of BD And were chosen as comparison stars. For the largest airmass during our observations, $X = 1.68$, the effect of the second-order extinction in the V passband is < 0.003 mag. For both telescopes the same set of comparison stars was used. A journal of the photometric observations is given in Table 1.

The heliocentric minima times determined by the Kwee & van Woerden (1956) method are listed in Table 1. The minima times are affected by the LC asymmetry, which is most marked in the B passband. For example, the egress from the minimum is considerably steeper on November 7, 2017, so the minimum of light occurs slightly earlier than the spectroscopic conjunction. LC was much more symmetric in 2018.

3. Broadening functions and radial velocities

Spectra of BD And were analyzed using the BF technique developed by Rucinski (1992). The BFs have been extracted in the 4900-5510 Å spectral range (free of hydrogen Balmer lines and telluric lines) for all three spectrographs. The

¹World Coordinate System

velocity step in the extracted BFs was set according to the spectral resolution. For eShel at G1 the step of $\Delta RV = 5.8 \text{ km s}^{-1}$ was used, for the MUSICOS and coudé échelle spectrograph at TLS, $\Delta RV = 3.5 \text{ km s}^{-1}$.

BFs were extracted using HD65583 (G8V) as the template. The extracted BFs clearly show three components: two rapidly-rotating components of the eclipsing pair and a slowly rotating third component (Fig. 1). The third component shows practically constant RV.

The BFs were first modeled by triple Gaussian functions. The model Gaussian profile corresponding to the third component was then subtracted from BFs. The BFs showing non-blended components were fitted by a double rotational profile (see Pribulla et al., 2015). The resulting RVs of the binary components are given in Appendix A. The rotational velocities of the components measured outside eclipses are $v_1 \sin i_1 = 69.0 \pm 0.7 \text{ km s}^{-1}$, $v_2 \sin i_2 = 68.8 \pm 1.2 \text{ km s}^{-1}$ for MUSICOS at SP, and $v_1 \sin i_1 = 70.8 \pm 1.2 \text{ km s}^{-1}$, $v_2 \sin i_2 = 70.7 \pm 0.8 \text{ km s}^{-1}$ for coudé échelle at TLS. The projected rotational velocity of the third component is below the spectral resolution, thus $v_3 \sin i_3 \leq 8 \text{ km s}^{-1}$. The slow rotation rate is a natural consequence of the magnetic breaking in a single late-type star.

The BFs extracted from the TLS and SP spectra are significantly less noisy and result in more precise RVs than those extracted from the G1 spectra. The RV of the third component derived from the SP and TLS spectroscopy is about -10.3 km s^{-1} . BFs from G1 clearly show the third component, but its profile is too noisy to determine the RV reliably.

Our spectroscopic observations resulted in 112 RVs for all three components. Because the time range of the observations is only about 3 years, the orbital period of the eclipsing pair was adopted from equation (2) of Kim et al. (2014). A circular orbit was assumed with the longitude of the periastron passage $\omega = \pi/2$. RVs of the primary and secondary component were modeled simultaneously. Errors of the RVs were estimated from equation (1) of Hatzes et al. (2010). Assuming the same rotational velocity and spectral range, we have:

$$\sigma_{RV} \propto \frac{1}{SNR R^{3/2}}, \quad (1)$$

where SNR is the signal-to-noise ratio and R is the spectral resolution. Having a sufficient number of spectra for every spectrograph, the RV errors were first derived from the signal-to-noise ratios as $1/SNR$. The errors were then re-scaled to give the reduced $\chi_r = 1$ for every spectrograph.

The scaling factors for eShel at G1 are 92 and 91 for the primary and secondary component, respectively. The scaling factors for MUSICOS at SP are 37 and 36 for the primary and secondary component, respectively. The scaling factors for coudé échelle at TLS are 33 and 74 for the primary and secondary component, respectively. After re-scaling the errors, all RVs were modeled simultaneously. The resulting best parameters are given in Table 2 and the corresponding fits are plotted in Fig. 2.

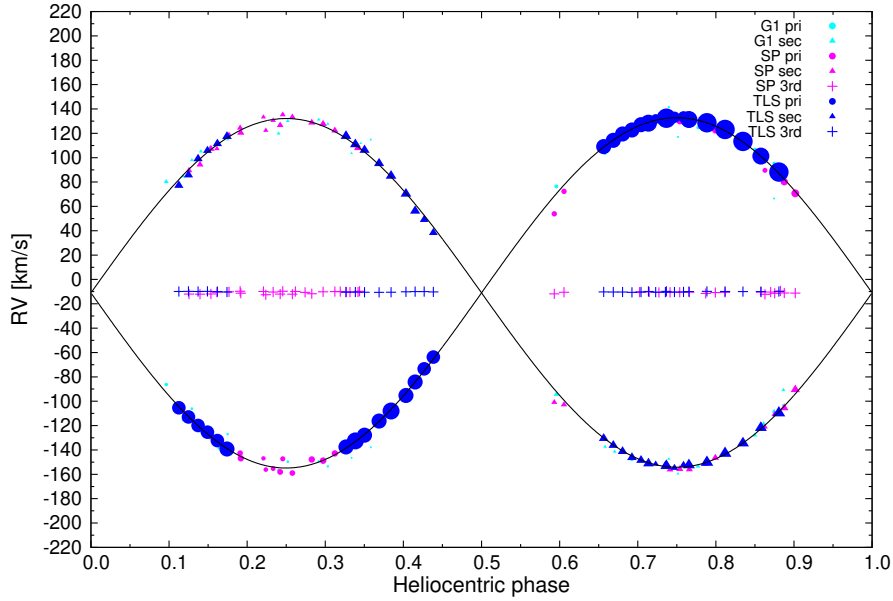


Figure 2. RV measurements of the primary, secondary and tertiary components of BD And and the corresponding Keplerian orbit fits. The point sizes scale with their weights ($1/\sigma^2$).

Using the inclination angle, $i = 92.72 \pm 0.19^\circ$, from Table 7 of Kim et al. (2014), one gets $M_1 = 1.135 \pm 0.006 M_\odot$ and $M_2 = 1.140 \pm 0.004 M_\odot$. While the mass of the primary component is close to the estimate of Kim et al. (2014), the secondary is about 13% more massive and the components are of equal mass within the margins of error. Our inclination angle $i = 86.48 \pm 0.04^\circ$ (see Section 5) gives the masses only by about 0.5% larger than the minimum masses provided by the spectroscopic orbits.

4. Timing variability and light-time effect

BD And shows periodic variability of the orbital period, indicating the presence of a third component in the system. Although the cyclic variability is clearly visible (see Fig. 3), the minima times are affected by the LC asymmetries resulting from dark photospheric spots. Moreover, the minima times were determined by different methods and obtained in different filters. Because the components are covered with cold spots (Kim et al., 2014), the spot effects are increasing in magnitude towards violet.

The observed-computed (O-C) diagram of Kim et al. (2014) shows that the older photographic and visual minima timings are unusable because of the large

Table 2. Spectroscopic elements of the primary and secondary components of BD And. The best fit is based on 112 RV measurements (30 from eShel, 50 from MUSICOS, and 32 from TLS).

Parameter	Value	σ
P [d]	0.92580526	–
T_0 [HJD]	2 457 931.1648	0.0003
V_0 [km s ⁻¹]	–11.11	0.13
K_1 [km s ⁻¹]	143.75	0.17
K_2 [km s ⁻¹]	143.24	0.29
$q = M_2/M_1$	1.0035	0.0024
$a_1 \sin i$ [R _⊙]	2.629	0.003
$a_2 \sin i$ [R _⊙]	2.620	0.005
$M_1 \sin^3 i$ [M _⊙]	1.132	0.005
$M_2 \sin^3 i$ [M _⊙]	1.136	0.004

scatter. Hence, we used CCD minima times only. In addition to the minima list of Kim et al. (2014) and our new observations, minima times were collected from publications of Parimucha et al. (2016), Hubscher (2015, 2017), Samolyk (2015a,b, 2018a,b, 2019a,b). Because of unsure and missing errors, two datasets were analyzed: (a) CCD minima with available error estimates (149 times), and (b) all CCD minima timings assuming the same errors/weights (164 times). In the latter case the error for all minima has been set to 0.0001 days. The observed minima times were modeled assuming a LiTE and a continuous period change:

$$\text{Min I} = T_{\text{min}} + P \times E + Q \times E^2 + \frac{a_{12} \sin i_{12}}{c} \left[\frac{1 - e_{12}^2}{1 + e_{12} \cos \nu_{12}} \sin(\nu_{12} + \omega_{12}) + e_{12} \sin \omega_{12} \right],$$

where $T_{\text{min}} + P \times E + Q \times E^2$ is the quadratic ephemeris of the eclipsing pair, $a_{12} \sin i_{12}$, e_{12} , ω_{12} , ν_{12} is the projected semi-major axis, the eccentricity, the longitude of periastron passage, and the true anomaly of the eclipsing-pair orbit around the common center of gravity, respectively. The data optimization was done assuming the linear ephemeris ($Q = 0$, i.e., a constant period) and quadratic ephemeris (a continuous period change with $dP/dt = \text{const}$) of the eclipsing pair.

The resulting reduced χ_r^2 for a continuous-period change are 31.1 and 71.1 for the first (a) and the second dataset (b), respectively. Very high χ_r^2 indicates that the published errors are underestimated or/and there is an additional intrinsic variability present in the timing data. To get reduced $\chi_r^2 \sim 1$ the mean observation error must be about 0.0008 days. The resulting parameters for both datasets are given in Table 3. The corresponding fit (all CCD minima, dataset b) together with predicted and observe systemic-velocity changes is shown in Fig. 3.

Table 3. The light-time orbit of the eclipsing pair around the common center of gravity with the third component. Reduced χ_r^2 is given. For dataset (b) $\sigma = 0.0008$ days was assumed for every datapoint. The time of the periastron passage, T_{12} , and the time of the minimum light, T_{\min} , are given without 2 400 000. The mass of the third component M_3 is given for $i_3 = 90^\circ$ (minimum mass).

Parameter	Dataset (a)	Dataset (a)	Dataset (b)	Dataset (b)
	quadratic	linear	quadratic	linear
T_{\min} [HJD]	34 962.846(9)	34 962.8696(9)	34 962.851(5)	34 962.8677(8)
P [day]	0.9258070(8)	0.92580489(4)	0.9258065(5)	0.92580496(3)
Q [day]	$-4.7(17) 10^{-11}$	–	$-3.7(11) 10^{-11}$	–
P_3 [day]	3299(37)	3259(31)	3358(26)	3324(18)
e_{12}	0.64(9)	0.58(7)	0.74(12)	0.70(10)
ω_{12} [deg]	296(7)	295(7)	308(6)	308(5)
T_{12} [HJD]	49 450(80)	49 510(80)	49 430(60)	49 490(40)
$a_{12} \sin i_{12}$ [a.u.]	0.78(6)	0.74(4)	0.86(13)	0.82(9)
$f(m)$ [M_\odot]	0.0057(13)	0.0051(9)	0.0077(34)	0.0068(21)
M_3 [M_\odot]	0.34(3)	0.33(3)	0.38(8)	0.36(4)
χ_r^2	31.1	32.4	1.111	1.180
d.o.f.	149-8	149-7	164-8	164-7

A hypothesis that the orbital period of the eclipsing pair is constant ($Q = 0$) was tested using the F-test for case (b) where more data are available. For the false-rejection probability of $\alpha = 0.05$ the critical value is $F = 3.9$, while the calculated value of the F statistics is 9.6. This means that the quadratic term is statistically significant. A possible cause for the observed period decrease in the eclipsing pair could be the angular momentum loss due to the magnetic braking. A very weak quadratic term was already found by Kim et al. (2014) from a shorter dataset (6984 vs. 9110 days). On the other hand, older photographic minima times² require a constant period of the eclipsing pair.

The LC asymmetry effect on the minima times can be estimated using formula (6) of Pribulla et al. (2012). Assuming an orbital period of $P = 0.9258$ days and parameters estimated from Fig. 8 of Kim et al. (2014), $D \sim 0.15P$ (minimum duration), $d \sim 0.4$ (eclipse depth), and $A_{\text{OCE}} \sim 0.05$ mag we get $\Delta t = 0.002$ days, which is comparable to the LiTE amplitude (see Fig. 3). This means that the LiTE orbit is rather unreliable and additional information on the LC asymmetry would be needed to disentangle the spot and LiTE effects to arrive at useful orbital elements.

5. Broadening-function and light-curve modeling

The LC analysis of BD And is complicated by the surface activity resulting in wave-like distortions. A detailed analysis of BVR photometry of the system was performed by Kim et al. (2014). Our photometry is inferior to their data because it was focused on obtaining the timing information. Another problem

²see e.g., <http://var2.astro.cz/ocgate/>

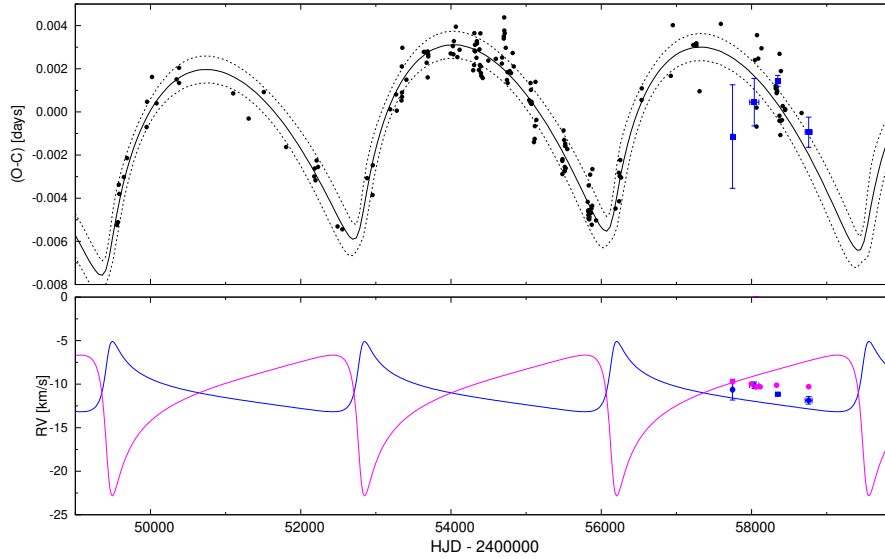


Figure 3. The O-C diagram for all available minima times of BD And (dataset a) with the best light-time effect model. The residuals are plotted for linear ephemeris $T_0 = \text{HJD } 2434962.87143 + 0.925804848 \times E$. The blue points correspond to the mean seasonal times of the spectroscopic conjunctions. One-sigma limits are plotted with dashed lines (top). The corresponding RV-change of the eclipsing pair and the third component is also shown together with seasonal mean values (bottom). The blue line corresponds to the mass center of the eclipsing pair and the magenta line to the third component.

is that the LC changes on the timescales as short as weeks or months. The only dataset obtained within a reasonably short time is the BI_c photometry from the G2 pavilion from August 3 till September 9, 2018. Unfortunately, the observations do not cover the maximum following the primary minimum. Our best available spectroscopy (TLS data) was obtained from July 27 till August 6, 2018, thus partially overlapping with these photometric data. BFs obtained after subtraction of the third component from the triple Gaussian model were used.

The simultaneous modeling of BFs and LCs was done using the code Roche (see Pribulla et al., 2018). The simultaneous analysis is crucial to lift the parameter degeneracies complicating even modeling of high-precision satellite LCs. Such is e.g. the correlation between the component radii and inclination angle (see Southworth et al., 2007).

Possible surface inhomogeneities were ignored due to the large phase gap in our photometric data preventing a sound analysis. The orbital period was

not adjusted but fixed at $P = 0.92580526$ days (see Kim et al., 2014). The following parameters are used T_0 - time of the periastron passage, P - orbital period, i - inclination angle, Ω_1 , Ω_2 - surface equipotentials, T_1 and T_2 polar temperatures of the primary and secondary component, l_3 - third light, l_{12} - LC normalization factor, spectroscopic elements - V_0 , $(K_1 + K_2)$ and BF background and normalization factors. The limb darkening was modeled using the linear limb-darkening law and tables of van Hamme (1993). The reflection effect and gravity darkening were computed assuming convective envelopes with $\beta_1 = \beta_2 = 0.08$, and $A_1 = A_2 = 0.5$. The component fluxes were computed using model atmosphere spectral energy distribution taking into account local gravity and temperature. The polar temperature of the primary was fixed at 5550 K as found from the infrared color indices (see Section 6). Third light was not adjusted and fixed at $l_3/(l_1 + l_2) = 0.1481$ in the B passband and $l_3/(l_1 + l_2) = 0.1933$ in the I_c passband corresponding the the results of Kim et al. (2014). A circular orbit and synchronous rotation of the components were assumed.

The BI_c LCs and their best fits are shown in Fig. 4. The best parameters are listed in Table 4. The modeling shows that the observations (especially the B data) show systematic deviations very probably caused by the surface inhomogeneities. We also note that the third light is strongly correlated to the inclination angle: the larger the third light the larger the inclination angle.

Obtaining a more reliable parameter set would require long-term monitoring of the system. Constructing the brightest LC (see Section 6 of Pribulla et al., 2001) could provide a better reference for the modeling of individual spot-affected LCs.

Table 4. Simultaneous modeling of BI_C light curves and broadening functions from the TLS spectra assuming all proximity effects using *Roche*. Luminosity uncertainties were computed assuming temperature errors of 100 K.

Parameter	<i>Roche</i>		Kim et al. (2014)	
		σ		σ
V_0 [km s $^{-1}$]	-11.11	0.12	-	-
$K_1 + K_2$ [km s $^{-1}$]	288.04	0.27	-	-
$q = M_2/M_1$	1.0017	0.0020	0.8770	0.0031
T_1 [K]	5550	-	5880	-
T_2 [K]	5522	3	5842	3
i [deg]	86.48	0.04	92.72	0.19
R_1 [R_\odot]	1.239	0.004	1.278	0.020
R_2 [R_\odot]	1.243	0.005	1.155	0.018
a [R_\odot]	5.281	0.004	5.152	0.055
M_1 [M_\odot]	1.152	0.003	1.145	0.053
M_2 [M_\odot]	1.154	0.003	1.001	0.047
L_1 [L_\odot]	1.31	0.09	1.75	0.19
L_2 [L_\odot]	1.29	0.09	1.39	0.15
$\log g_1$ [cgs]	4.313	0.003	4.284	0.024
$\log g_2$ [cgs]	4.311	0.004	4.314	0.024

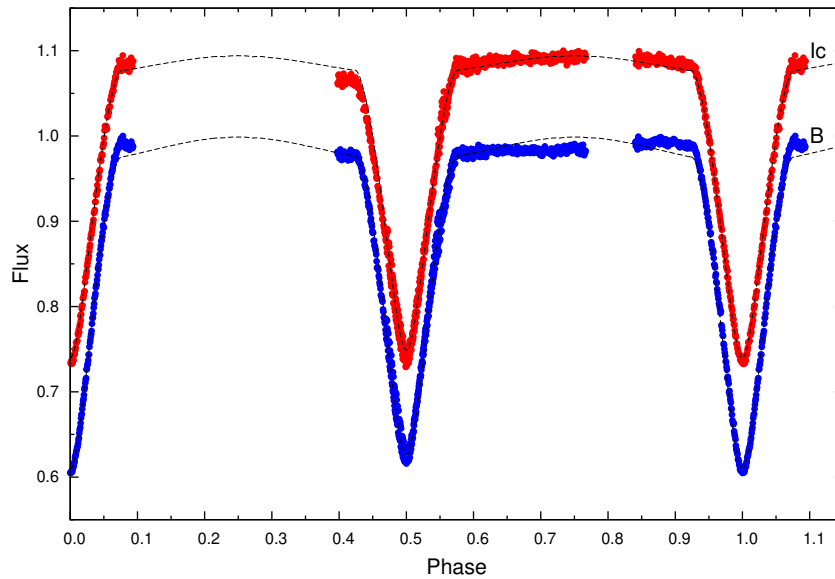


Figure 4. *BI* light curves of BD And obtained from August 3 till September 9, 2018 and their best fits resulting from the simultaneous modeling of light curves and broadening functions.

6. Third component and the outer orbit

The existence of a third component on a long-period orbit was first indicated by the timing variability and third light in the LC modeling (see Sipahi & Dal, 2014). Our new spectroscopy conclusively shows the presence of an additional component.

The light contribution of the third component, $l_3/(l_1 + l_2)$, determined from the Gaussian-function multi-profile fit is 0.213 ± 0.005 (observations in an eclipsing-binary phase interval from 0.163 to 0.344). This means that the 3rd component is slightly later than the components of the eclipsing binary. The light contribution of the components in the spectrum reflects the relative strength of metallic lines (mostly Fe I, Fe II, Mg I). Because the 3rd component is of a later spectral type than the eclipsing binary and the metallic-line strength increases from G to K spectral types, the determined third light is overestimated. To correct this effect, the dependence of BF strength on $(B - V)$ for the solar metallicity from Table 3 of Rucinski et al. (2013) was used. Assuming that the binary components are of G1V spectral type and the third component is of G7V type (Kim et al., 2014, Tables 8 and 10) and that the metallicity of all three stars is the same, the correction factor is 0.838. Thus the third-light contribution is $l_3/(l_1 + l_2) = 0.178 \pm 0.004$ or $l_3/(l_1 + l_2 + l_3) = 0.151 \pm 0.004$ in the spectral

range where BFs were extracted (4900-5400Å). This is in a good agreement with the photometrically-determined value $l_3/(l_1 + l_2 + l_3) = 0.143 \pm 0.006$ in the V passband (Kim et al., 2014).

The observed combined infrared color of BD And is $J - K = 0.449 \pm 0.026$. If we neglect the interstellar reddening (see Kim et al., 2014), this corresponds to a G6-7V spectral type with one sub-type uncertainty or $T_{\text{eff}} = 5550 \pm 100$ K (Cox, 2000). If all three stars are main-sequence objects, the observed infrared color can be obtained having two components of the G5V spectral type and a late-type companion of the K2V spectral type. Then the combined infrared color is $J - K = 0.446$ and third light is $l_3/(l_1 + l_2) = 0.151$, which is a bit less than our spectroscopic determination $l_3/(l_1 + l_2) = 0.178$. Combining two main-sequence components of G6V spectral type and a K2V main-sequence star results in $l_3/(l_1 + l_2) = 0.171$, but with a slightly redder combined color $J - K = 0.464$. The late spectral types of the components indicated by the infrared color are, however, inconsistent with their masses, if they are main-sequence objects.

The predicted 9-year orbital revolution of the eclipsing pair around the common center of gravity is expected to cause changes of its systemic velocity. To get some constraint on the outer orbit, the RVs were divided into individual observing seasons. We kept RV semi-amplitudes, K_1, K_2 , of the components fixed, varying only the time of the spectroscopic conjunction, T_0 , and systemic velocity, V_0 . Resulting systemic velocities are $V_0 = -10.63 \pm 1.19$ km s⁻¹ (2016/2017), $V_0 = -10.13 \pm 0.38$ km s⁻¹ (2017/2018), $V_0 = -11.16 \pm 0.13$ km s⁻¹ (2018/2019), and $V_0 = -11.86 \pm 0.43$ km s⁻¹ (2019/2020). The average RV of the third component per season and instrument was also computed³. The resulting RV data and the timing of the spectroscopic conjunction are plotted in the (O-C) diagram in Fig. 3.

The systemic velocity and RV of the third component were observed to be identical within about 1-2 km s⁻¹ and so $V_0 \sim V_3$. This practically confirms the gravitational bond of the third component to the eclipsing pair. The observed systemic RV changes (see Section 3) of the eclipsing pair and the third component are, however, inconsistent with the LiTE orbit. The predicted RV difference depends on the mass ratio $M_3/(M_1 + M_2)$. Assuming that $M_3/(M_1 + M_2) = 0.41$ (Kim et al., 2014), the LiTE fit predicts the RV difference to decrease from $V_0 - V_3 = -1.8$ km s⁻¹ to $V_0 - V_3 = -5.5$ km s⁻¹ during our spectroscopy, which is not observed. While the third component shows a constant velocity, the systemic velocity of the eclipsing pair seems to be slowly decreasing. This means that (i) the timing variability is caused by the LiTE but the determination of ω_{12} or/and e_{12} is incorrect and affected by the LC asymmetries, or (ii) the component causing the timing variability is not visible in the spectra. In the latter case, the body which causes the timing variability and eclipsing

³The only deviating point is the RV obtained from the MUSICOS data in the 2018/2019 season when better observations were obtained at TLS. This point was excluded from further considerations.

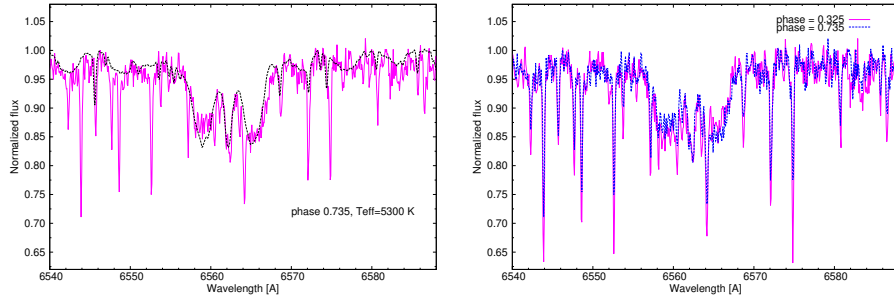


Figure 5. Comparison of the observed H_{α} line profile (TLS spectrum from HJD 2 458 336.42400) and the synthetic spectrum for $T_{\text{eff}} = 5300$ K convolved with corresponding BF at phase $\phi = 0.735$ (right). The bottom plot shows comparison of two spectra obtained at TLS at $\phi = 0.325$ (HJD 2 458 330.48948) and $\phi = 0.735$ (HJD 2 458 336.42400).

binary systemic velocity changes must be an intrinsically faint object unseen in the spectra.

A more reliable characterization of the third component would require spectroscopic observations covering the entire long-period orbit. An important requirement is the long-term RV stability of the instrument(s) at the level of at least 100-200 m s^{-1} .

7. Surface activity

BD And is composed of two solar-like components. Unlike our Sun, the components are fairly fast rotators with projected rotational velocities about 70 km s^{-1} . Thus one can expect enhanced photospheric and chromospheric activity.

The best indicator of the surface activity are chromospheric lines Ca II H and K, H_{α} and Ca IRT (see e.g., Eker et al., 1995; Biazzo et al., 2006; Zhang et al., 2015). Our spectroscopic observations cover only H_{α} . In chromospherically active stars H_{α} has typically a lower equivalent width (EQW) compared to that expected for the given spectral type. To determine the extra emission, synthetic spectra have been calculated using code iSpec (Blanco-Cuaresma et al., 2014a,b) assuming various effective temperatures $T_{\text{eff}} = 5100, 5300, 5500$ and 5700 K, the Solar metallicity, $\log g = 4.3$ [cgs] and the microturbulent velocity $\xi = 2 \text{ km s}^{-1}$. The synthetic spectra were then convolved with extracted BFs. The resulting convolved synthetic spectra for $T_{\text{eff}} \leq 5500$ K match the depth of the observed H_{α} line profile very well and do not indicate any extra emission (see Fig. 5). On the other hand, for two components of the same brightness and temperature as indicated by the combined LC and BF solution and practically equal masses (Section 3) we see different line depth (Fig. 5, bottom). The EQW is higher for

the primary component. This indicates some surface activity on the secondary component lowering its EQW.

We searched for direct spot signatures in the BFs extracted from the TLS high-dispersion and high SNR spectroscopy. The third component, represented by a model Gaussian function, was subtracted. The BFs were extracted from metallic lines not affected by chromospheric activity. To enhance the spots in BFs, their best fits by the Roche-code modeling (see Section 3) were subtracted. The resulting residuals (Fig. 6) do not conclusively show the presence of spots. The analysis of BD And is, however, complicated by the presence the third component which cannot be completely subtracted. Moreover, the observed profiles of the components do not perfectly follow the theoretical predictions based on the solid-body rotation.

8. Discussion and conclusions

Extensive échelle spectroscopy conclusively showed that eclipsing binary BD And is part of a hierarchical triple system. The RVs of all three components were determined using the BF technique appropriate for heavily broadened spectra of close binaries. The power of this deconvolution method is documented by the fact that useful RVs were determined even from low SNR spectra obtained with a 60cm telescope.

The eclipsing pair is composed of two almost identical solar-type components accompanied by a late-type star. Throughout our observations the third component showed a constant RV very close to the systemic velocity of the binary, strongly supporting the gravitational bond. The orbital motion in the outer, 9-year orbit indicated by the timing variability could not be detected spectroscopically. The difference of the systemic velocity of the eclipsing pair and RV of the third component is inconsistent with the outer orbit based on the timing information. The minima times are probably shifted from spectroscopic conjunction by the surface spot activity. This negatively influences the determination of the orbital elements. Hence, future photometric observations should be obtained in the *I* passband least affected by the spots but still accessible by silicon-based CCDs. Having both primary and secondary minima observed within a couple of days is also important. This would enable one to better quantify the spot effects on the timing information.

The identification of the third component seen in the BFs extracted from visual spectroscopy with the additional component indicated by the timing variability is spurious. The minimum mass of the third component found from the LiTE modeling ranges from 0.33 to 0.38 M_{\odot} . If it is a main-sequence star on an edge-on orbit, its light contribution would be <1% (see Xia et al., 2008). Then the component seen in spectra is another star on a much wider orbit.

The projected semi-major axis of the eclipsing pair around the common center of gravity found from minima timing is $a_{12} \sin i_{12} = 0.86 \pm 0.13$ a.u. (case b

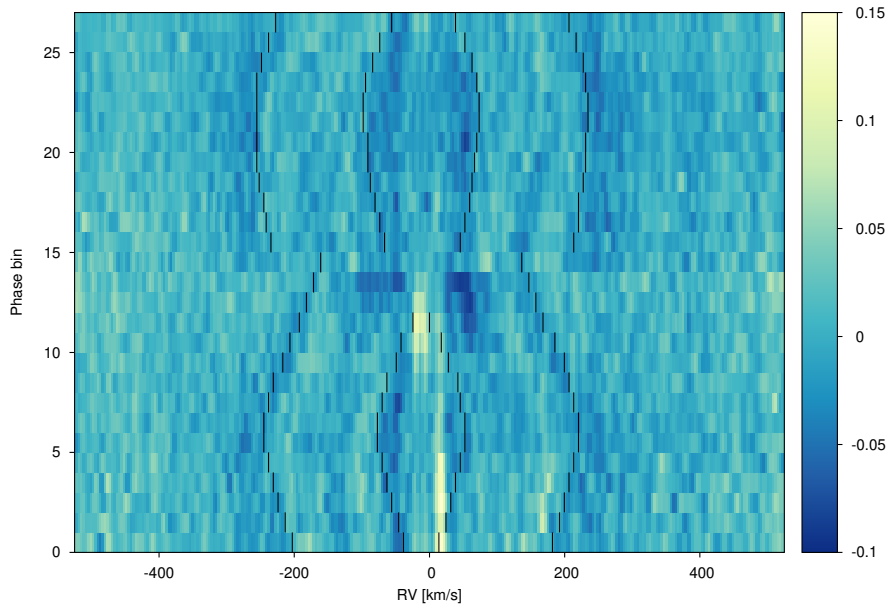


Figure 6. Residuals from the BF fitting. Only TLS observations are plotted. The RV span of both components is indicated by solid black lines. The corresponding orbital-phase ranges (from bottom) are 0.111-0.173 (6 rows), 0.325-0.437 (9 rows) and 0.655-0.879 (13 rows). Only spectra from July/August 2018 are shown.

with quadratic ephemeris). The corresponding systemic velocity of the eclipsing pair is predicted to range from -1.8 km s^{-1} to $+5.5 \text{ km s}^{-1}$. Such RV variability should easily be detected even with modest spectrographs. Long-term spectroscopic observations are crucial to determine the outer-orbit elements and mutual inclination of the inner and outer orbit. Of special importance is the determination of the mass ratio $M_3/(M_1 + M_2)$.

Interferometric observations would be hard to perform because of the low brightness of the system ($J = 9.504 \pm 0.022$, $H = 9.164 \pm 0.021$, $K = 9.055 \pm 0.014$, 2MASS) even if the expected maximum separation of the eclipsing pair is about 20 mas (see Kim et al., 2014).

The unusable trigonometric parallax from Gaia DR2 (Gaia Collaboration et al., 2018), $\pi = 0.13 \pm 0.63 \text{ mas}$ is, very probably, resulting from the perturbations of an additional component (e.g., variability induced motion). It is, however, possible, that the astrometric motion will be taken into account in the final data release. In order to check the distances, we derived X-ray luminosities from the ROSAT catalog by converting count rate and hardness ratio into a physical flux with the method described by Schmitt et al. (1995). The resulting flux, as well those from the Swift and XMM-Newton observations, were then converted into luminosities by assuming the distances in question. For a dis-

tance of 294 pc (Kim et al., 2014), this yields $L_X^{\text{RASS}} = (7.2 \pm 1.9) \cdot 10^{30}$ erg/s, $L_X^{\text{Swift}} = (2.8 \pm 1.1) \cdot 10^{31}$ erg/s and $L_X^{\text{XMM}} = (1.5 \pm 0.5) \cdot 10^{31}$ erg/s, which corresponds to $\log(L_X/L_{\text{bol}}) = -3.3$, -2.7 and -2.97 , respectively. The resulting X-ray luminosities are in good agreement with each other and indicate that the system is highly active at the saturation limit of $\log(L_X/L_{\text{bol}}) = -3$. This also indicates that a distance larger than ~ 300 pc is physically implausible, since it would implicate that all of the components of BD And are above the saturation limit.

Acknowledgements. The authors thank V. Kollár for his technical assistance. This work has been supported by the VEGA grant of the Slovak Academy of Sciences No. 2/0031/18, by the Slovak Research and Development Agency under the contract No. APVV-015-458. This work was also supported by the GINOP 2.3.2-15-2016-00003 of the Hungarian National Research, Development and Innovation Office and the City of Szombathely under Agreement No. 67.177-21/2016. This research has made use of NASA's Astrophysics Data System and the SIMBAD database, operated at CDS, Strasbourg, France. The authors thank an anonymous referee for his/her constructive comments.

References

- Applegate, J., A mechanism for orbital period modulation in close binaries. 1992, *Astrophys. J.*, **385**, 621, DOI: 10.1086/170967
- Baudrand, J. & Bohm, T., MUSICOS - A fiber-fed spectrograph for multi-site observations. 1992, *Astron. Astrophys.*, **259**, 711
- Biazzo, K., Frasca, A., Catalano, S., & Marilli, E., Photospheric and chromospheric active regions on three single-lined RS CVn binaries. 2006, *Astron. Astrophys.*, **446**, 1129, DOI: 10.1051/0004-6361:20053213
- Blanco-Cuaresma, S., Soubiran, C., Heiter, U., & Jofré, P., Determining stellar atmospheric parameters and chemical abundances of FGK stars with iSpec. 2014a, *Astron. Astrophys.*, **569**, A111, DOI: 10.1051/0004-6361/201423945
- Blanco-Cuaresma, S., Soubiran, C., Jofré, P., & Heiter, U., iSpec: An integrated software framework for the analysis of stellar spectra. 2014b, in *Astronomical Society of India Conference Series*, Vol. **11**, *Astronomical Society of India Conference Series*
- Carter, J., Fabrycky, D., Ragozzine, D., et al., KOI-126: A Triply Eclipsing Hierarchical Triple with Two Low-Mass Stars. 2011, *Science*, **331**, 562, DOI: 10.1126/science.1201274
- Cox, A. 2000, *Allen's astrophysical quantities* (Springer-Verlag, New York)
- Eker, Z., Hall, D. S., & Anderson, C. M., H alpha Profiles of 25 Chromospherically Active Binaries. 1995, *Astrophys. J., Suppl.*, **96**, 581, DOI: 10.1086/192129
- Evans, P., Osborne, J., Beardmore, A., et al., VizieR Online Data Catalog: 1SXPS Swift X-ray telescope point source catalogue (Evans+ 2014). 2013, *VizieR Online Data Catalog*, IX/43

- Florja, N. 1938, *Peremennye Zvezdy*, **5**, 299
- Gaia Collaboration, Brown, A. G. A., Vallenari, A., et al., Gaia Data Release 2. Summary of the contents and survey properties. 2018, *Astron. Astrophys.*, **616**, A1, DOI: 10.1051/0004-6361/201833051
- Guenther, E., Hartmann, M., Esposito, M., et al., A substellar component orbiting the F-star 30 Arietis B. 2009, *Astron. Astrophys.*, **507**, 1659, DOI: 10.1051/0004-6361/200912112
- Hartmann, M., Guenther, E., & Hatzes, A., A Sub-stellar Companion around the F7 V Star HD 8673. 2010, *Astrophys. J.*, **717**, 348, DOI: 10.1088/0004-637X/717/1/348
- Hatzes, A., Cochran, W., & Endl, M., The Detection of Extrasolar Planets Using Precise Stellar Radial Velocities. 2010, in *Astrophysics and Space Science Library*, Vol. **366**, *Planets in Binary Star Systems*, ed. N. Haghighipour, 51
- Hatzes, A., Guenther, E., Endl, M., et al., A giant planet around the massive giant star HD 13189. 2005, *Astron. Astrophys.*, **437**, 743, DOI: 10.1051/0004-6361:20052850
- Hubscher, J., BAV-Results of observations - Photoelectric Minima of Selected Eclipsing Binaries and Maxima of Pulsating Stars. 2015, *Information Bulletin on Variable Stars*, **6152**
- Hubscher, J., BAV-Results of observations - Photoelectric Minima of Selected Eclipsing Binaries and Maxima of Pulsating Stars. 2017, *Information Bulletin on Variable Stars*, **6196**, DOI: 10.22444/IBVS.6196
- Kim, C.-H., Song, M.-H., Yoon, J.-N., Han, W., & Jeong, M.-J., BD Andromedae: A New Short-period RS CVn Eclipsing Binary Star with a Distant Tertiary Body in a Highly Eccentric Orbit. 2014, *Astrophys. J.*, **788**, 134, DOI: 10.1088/0004-637X/788/2/134
- Kozai, Y., Secular perturbations of asteroids with high inclination and eccentricity. 1962, *Astron. J.*, **67**, 591, DOI: 10.1086/108790
- Kwee, K. & van Woerden, H., A method for computing accurately the epoch of minimum of an eclipsing variable. 1956, *Bull. Astron. Inst. Netherlands*, **12**, 327
- Parenago, N. 1938, *Peremennye Zvezdy*, **5**, 157
- Parimucha, Š., Dubovský, P., Kudak, V., & Perig, V., Minima Times of Selected Eclipsing Binaries. 2016, *Information Bulletin on Variable Stars*, **6167**
- Pribulla, T., Baluďanský, D., Dubovský, P., et al., VW LMi: tightest quadruple system known. Light-time effect and possible secular changes of orbits. 2008, *Mon. Not. R. Astron. Soc.*, **390**, 798, DOI: 10.1111/j.1365-2966.2008.13781.x
- Pribulla, T., Chochol, D., Heckert, P., et al., An active binary XY UMa revisited. 2001, *Astron. Astrophys.*, **371**, 997, DOI: 10.1051/0004-6361:20010459
- Pribulla, T., Garai, Z., Hambálek, L., et al., Affordable échelle spectroscopy with a 60 cm telescope. 2015, *Astronomische Nachrichten*, **336**, 682, DOI: 10.1002/asna.201512202
- Pribulla, T., Mérand, A., Kervella, P., et al., Physical parameters and $\pm 0.2\%$ parallax of the detached eclipsing binary V923 Scorpii. 2018, *Astron. Astrophys.*, **616**, A49, DOI: 10.1051/0004-6361/201730673

- Pribulla, T. & Rucinski, S., Contact Binaries with Additional Components. I. The Extant Data. 2006, *Astron. J.*, **131**, 2986, DOI: 10.1086/503871
- Pribulla, T., Rucinski, S., Lu, W., et al., Radial Velocity Studies of Close Binary Stars. XI. 2006, *Astron. J.*, **132**, 769, DOI: 10.1086/505536
- Pribulla, T., Vaňko, M., Ammler-von Eiff, M., et al., The Dwarf project: Eclipsing binaries - precise clocks to discover exoplanets. 2012, *Astronomische Nachrichten*, **333**, 754, DOI: 10.1002/asna.201211722
- Pych, W., A Fast Algorithm for Cosmic-Ray Removal from Single Images. 2004, *Publ. Astron. Soc. Pac.*, **116**, 148, DOI: 10.1086/381786
- Rappaport, S., Deck, K., Levine, A., et al., Triple-star Candidates among the Kepler Binaries. 2013, *Astrophys. J.*, **768**, 33, DOI: 10.1088/0004-637X/768/1/33
- Rucinski, S., Spectral-line broadening functions of WUMa-type binaries. I - AW UMa. 1992, *Astron. J.*, **104**, 1968, DOI: 10.1086/116372
- Rucinski, S., Pribulla, T., & Budaj, J., Spectroscopic Metallicity Determinations for W UMa-type Binary Stars. 2013, *Astron. J.*, **146**, 70, DOI: 10.1088/0004-6256/146/3/70
- Samolyk, G., Recent Minima of 149 Eclipsing Binary Stars. 2015a, *Journal of the American Association of Variable Star Observers (JAAVSO)*, **43**, 77
- Samolyk, G., Recent Minima of 171 Eclipsing Binary Stars. 2015b, *Journal of the American Association of Variable Star Observers (JAAVSO)*, **43**, 238
- Samolyk, G., Recent Minima of 172 Eclipsing Binary Stars. 2018a, *Journal of the American Association of Variable Star Observers (JAAVSO)*, **46**, 79
- Samolyk, G., Recent Minima of 266 Eclipsing Binary Stars. 2018b, *Journal of the American Association of Variable Star Observers (JAAVSO)*, **46**, 184
- Samolyk, G., Recent Minima of 200 Eclipsing Binary Stars. 2019a, *Journal of the American Association of Variable Star Observers (JAAVSO)*, **47**, 265
- Samolyk, G., Recent Minima of 242 Eclipsing Binary Stars. 2019b, *Journal of the American Association of Variable Star Observers (JAAVSO)*, **47**, 106
- Schmitt, J., Fleming, T., & Giampapa, M., The X-Ray View of the Low-Mass Stars in the Solar Neighborhood. 1995, *Astrophys. J.*, **450**, 392, DOI: 10.1086/176149
- Shaw, J., Caillault, J.-P., & Schmitt, J., Near-Contact Binary Systems in the ROSAT All-Sky Survey. 1996, *Astrophys. J.*, **461**, 951, DOI: 10.1086/177116
- Sipahi, E. & Dal, H., A γ Doradus candidate in eclipsing binary BD And? 2014, *New Astronomy*, **26**, 62, DOI: 10.1016/j.newast.2013.06.001
- Southworth, J., Bruntt, H., & Buzasi, D., Eclipsing binaries observed with the WIRE satellite. II. β Aurigae and non-linear limb darkening in light curves. 2007, *Astron. Astrophys.*, **467**, 1215, DOI: 10.1051/0004-6361:20077184
- Thizy, O. & Cochard, F., Spectrographs for small telescopes. 2011, in IAU Symposium, Vol. **272**, *Active OB Stars: Structure, Evolution, Mass Loss, and Critical Limits*, ed. C. Neiner, G. Wade, G. Meynet, & G. Peters, 282–283

- Tokovinin, A., Mason, B., & Hartkopf, W., Speckle Interferometry at the Blanco and SOAR Telescopes in 2008 and 2009. 2010, *Astron. J.*, **139**, 743, DOI: 10.1088/0004-6256/139/2/743
- van Hamme, W., New Limb-Darkening Coefficients for Modeling Binary Star Light Curves. 1993, *Astron. J.*, **106**, 2096, DOI: 10.1086/116788
- Xia, F., Ren, S., & Fu, Y., The empirical mass-luminosity relation for low mass stars. 2008, *Astrophys. Space Sci.*, **314**, 51, DOI: 10.1007/s10509-007-9729-8
- XMM-SSC, VizieR Online Data Catalog: XMM-Newton slew survey Source Catalogue, version 2.0 (XMM-SSC, 2017). 2018, *VizieR Online Data Catalog*, IX/53
- Zhang, L.-Y., Pi, Q.-F., & Zhu, Z.-Z., Chromospheric activity in several single late-type stars. 2015, *Research in Astronomy and Astrophysics*, **15**, 252, DOI: 10.1088/1674-4527/15/2/009

A. Radial-velocity observations

Table 5. Journal of spectroscopic observations of BD And. The table gives heliocentric Julian date, barycentric RVs for all three components, signal-to-noise ratio and the instrument used. The instruments are: G1 - eShel spectrograph in G1 pavilion at Stará Lesná, SP - MUSICOS spectrograph at Skalnaté Pleso, TLS - Coudé échelle at Tautenburg. Only observations where radial velocities of all three components could be determined are listed. The computer readable form of these data can be found at: <https://www.astro.sk/caosp/Eedition/FullTexts/vol50no3/pp649-671.dat/>.

HJD −2 400 000	RV ₁ [km s ^{−1}]	RV ₂ [km s ^{−1}]	RV ₃ [km s ^{−1}]	SNR	Inst.
57727.17144	103.3	−137.4	−7.9	13	G1
57727.18283	112.5	−141.4	−8.8	14	G1
57727.19328	115.6	−140.4	−10.0	15	G1
57753.16967	141.4	−147.4	−14.7	12	G1
57753.18048	117.1	−159.5	−12.8	10	G1
57753.19241	132.9	−153.9	−14.8	13	G1
57753.20425	124.7	−153.5	−12.7	17	G1
57754.19736	106.8	−128.0	−6.8	17	G1
57754.20782	102.0	−118.7	−8.0	17	G1
57754.22026	95.3	−108.4	−4.0	16	G1
57754.23120	90.0	−90.8	−6.5	14	G1
57966.56809	−156.5	119.8	−14.0	14	G1
57966.57901	−149.7	130.1	−2.9	13	G1
57968.50619	−146.5	103.6	−4.9	10	G1
57968.51727	−131.1	111.8	−10.7	10	G1
57968.52890	−137.8	114.8	−8.3	10	G1
57987.51260	100.9	−121.2	−10.8	11	G1
57987.52308	66.5	−108.4	−19.9	10	G1
57987.53357	93.3	−103.3	−9.0	10	G1
57991.45162	−115.3	84.6	−13.2	14	G1
57991.46211	−106.1	98.0	−13.6	13	G1
57991.47276	−124.8	105.1	−10.1	14	G1
57991.48326	−130.3	108.2	−9.4	14	G1
57991.49389	−138.6	112.3	−8.2	13	G1
57991.50444	−127.1	114.9	−9.0	12	G1
57992.53812	−149.3	131.2	−12.5	12	G1
57992.54905	−153.5	127.7	−11.8	12	G1
58028.46393	−86.2	80.2	−9.6	17	G1
58073.36486	76.4	−94.5	−8.2	19	G1
58113.26396	127.6	−148.5	−3.4	11	G1
58060.52132	131.8	−151.6	−10.4	24	TLS
58060.53281	132.5	−152.4	−10.4	29	TLS
58060.54355	133.2	−154.8	−10.3	28	TLS
58060.55429	133.5	−152.3	−10.2	28	TLS
58081.29493	−129.9	107.3	−10.5	12	SP

Table 5. Continued.

HJD -2 400 000	RV ₁ [km s ⁻¹]	RV ₂ [km s ⁻¹]	RV ₃ [km s ⁻¹]	SNR	Inst.
58081.30922	-139.9	118.8	-10.1	12	SP
58081.32243	-142.6	124.3	-9.7	13	SP
58134.17812	-147.8	128.7	-11.7	15	SP
58134.19155	-148.7	127.6	-10.1	16	SP
58134.20553	-142.8	122.2	-10.0	15	SP
58134.21896	-136.1	118.3	-10.2	17	SP
58134.23299	-130.6	107.9	-10.3	17	SP
58327.51391	-105.4	77.1	-9.9	33	TLS
58327.52534	-112.9	85.7	-9.8	35	TLS
58327.52599	-112.7	89.4	-12.0	14	SP
58327.53668	-119.9	99.0	-9.9	34	TLS
58327.53901	-121.6	94.2	-12.1	15	SP
58327.54786	-125.4	105.7	-9.8	33	TLS
58327.55192	-128.6	107.1	-11.9	16	SP
58327.55964	-132.3	111.4	-10.0	33	TLS
58327.57104	-139.2	117.3	-10.3	35	TLS
58328.51309	-146.8	120.3	-11.3	15	SP
58328.54287	-156.1	122.3	-12.5	11	SP
58328.55978	-158.1	126.5	-12.0	14	SP
58328.57425	-159.0	133.3	-12.1	14	SP
58330.48948	-137.5	117.6	-10.4	38	TLS
58330.50053	-132.6	110.8	-10.3	39	TLS
58330.51137	-127.9	106.1	-10.5	38	TLS
58330.52868	-116.3	95.2	-10.6	38	TLS
58330.54287	-108.0	84.9	-10.5	39	TLS
58331.48629	-95.3	70.2	-10.1	38	TLS
58331.49716	-84.2	56.1	-10.0	37	TLS
58331.50795	-73.4	49.0	-10.0	32	TLS
58331.51879	-63.7	38.3	-10.2	32	TLS
58334.49805	109.1	-130.6	-10.2	36	TLS
58334.50951	114.2	-136.3	-10.3	36	TLS
58334.52045	119.5	-141.3	-10.3	36	TLS
58334.53156	122.7	-146.3	-10.6	36	TLS
58334.54239	127.1	-148.6	-10.3	36	TLS
58336.40274	128.3	-151.3	-9.9	39	TLS
58336.42400	132.4	-153.2	-9.8	45	TLS
58336.45072	131.3	-152.6	-10.0	44	TLS
58336.47203	128.7	-150.4	-9.8	47	TLS
58336.49351	123.2	-143.0	-9.9	46	TLS
58336.51476	113.3	-134.6	-10.0	44	TLS
58336.53603	101.3	-121.9	-10.0	43	TLS
58336.55729	88.2	-109.8	-10.0	46	TLS
58358.51050	53.9	-100.9	-11.8	13	SP
58358.52196	72.3	-102.9	-10.5	13	SP

Table 5. Continued.

HJD -2 400 000	RV ₁ [km s ⁻¹]	RV ₂ [km s ⁻¹]	RV ₃ [km s ⁻¹]	SNR	Inst.
58360.49929	128.3	-156.2	-10.6	14	SP
58360.51073	129.9	-155.8	-10.5	15	SP
58360.52220	135.3	-156.0	-10.4	15	SP
58360.54154	129.1	-151.8	-11.5	14	SP
58360.55300	122.5	-146.6	-10.8	16	SP
58360.56446	121.1	-142.5	-10.6	14	SP
58374.49887	89.6	-121.2	-12.2	12	SP
58374.51033	88.0	-110.7	-11.4	13	SP
58374.52179	80.2	-105.6	-11.1	18	SP
58374.53482	70.7	-90.6	-11.2	19	SP
58431.30439	-146.9	133.3	-9.9	11	SP
58431.31585	-155.3	130.5	-10.3	12	SP
58431.32732	-147.3	135.2	-9.7	12	SP
58431.34228	-153.1	127.9	-9.9	10	SP
58431.35374	-150.8	131.5	-10.6	9	SP
58705.43381	-140.9	117.5	-10.0	11	SP
58705.44527	-137.6	110.3	-10.4	11	SP
58705.45672	-127.6	106.6	-9.7	11	SP
58721.52721	125.2	-149.1	-10.4	15	SP
58721.53866	127.7	-151.5	-10.2	15	SP
58721.55013	131.1	-153.5	-10.7	15	SP
58723.52282	97.3	-120.7	-10.4	13	SP
58723.53427	89.8	-113.0	-10.3	13	SP
58781.38578	-119.9	100.4	-10.5	17	SP
58781.39911	-116.7	89.1	-10.5	17	SP
58781.41057	-106.1	82.7	-10.1	17	SP
58795.31985	-89.0	67.8	-9.8	10	SP
58811.25235	90.3	-110.1	-10.8	10	SP
58811.26380	92.8	-122.4	-10.5	13	SP
58811.27524	102.8	-122.0	-10.3	13	SP
58823.25516	61.4	-85.3	-10.8	15	SP
58823.26662	70.9	-98.0	-10.2	15	SP

LAMOST J202629.80+423652.0 is not a symbiotic star

V. Andreoli¹ and U. Munari²

¹ *ANS Collaboration, Astronomical Observatory, 36012 Asiago (VI), Italy*

² *INAF Padova Astronomical Observatory, I-36012 Asiago (VI), Italy*

Received: March 24, 2020; Accepted: April 15, 2020

Abstract. LAMOST J202629.80+423652.0 has been recently classified as a new symbiotic star containing a long-period Mira, surrounded by dust (D-type) and displaying in the optical spectra high ionization emission lines, including the Raman-scattered OVI at 6825 Å. We have observed LAMOST J202629.80+423652.0 photometrically in the BVRI bands and spectroscopically over the 3500-8000 Å range. We have found it to be a normal G8IV sub-giant star, deprived of any emission line in its spectrum, and reddened by $E_{B-V}=0.35$ mag. Combining our photometry with data from all-sky patrol surveys, we find LAMOST J202629.80+423652.0 to be non variable, so not pulsating as a Mira. We have compiled from existing sources its spectral energy distribution, extending well into the mid-Infrared, and found it completely dominated by the G8IV photospheric stellar emission, without any sign of circumstellar dust. We therefore conclude that LAMOST J202629.80+423652.0 is not a symbiotic star, nor it is pulsating or been enshrouded in dust.

Key words: binaries: symbiotic – surveys: LAMOST

1. Introduction

Symbiotic stars (SySt) are binary systems composed by a red giant star (RG) that transfers material to a degenerate companion which can be either a white dwarf (WD) or a neutron star (NS). SySt are broadly divided into two major groups (see the recent review by Munari 2019): those *accreting-only* whose optical spectra are dominated by the RG with no or weak emission lines, and the *burning-type* displaying a strong nebular continuum and a rich emission line spectrum: they originate in the wind of the RG largely ionized by the very hot and luminous WD companion that is nuclearly burning at the surface in stable conditions. The accreting-only SySt usually requires satellite UV/X-ray observations to be discovered (cf. the prototype SU Lyn, Mukai et al. 2016), while the burning StSy can easily be discovered through the whole Galaxy and the Local Group thanks to the prominent emission lines. In about 20% of the known SySt (see recent catalogs of symbiotic stars by Belczyński et al. 2000, and Akras et al. 2019), the cool giant pulsates as a Mira and this usually comes also with the

presence of warm circumstellar dust ($\sim 500\text{--}1000$ K), leading to a classification as D-type according to the scheme introduced by Allen (1982).

Li et al. (2015) have announced the discovery of two new SySt during the LAMOST all-sky spectroscopic survey. LAMOST is a 4m Schmidt telescope located in Xinglong (China), feeding light to 16 spectrographs via 4000 optical fibers. The spectrum presented by Li et al. for one of these two new SySt, namely LAMOST J202629.80+423652.0 (hereafter LM), looks weird and we suspected to be the result of problematic sky subtraction, so decided to investigate the matter by acquiring new spectra and supplementing them with acquisition of BVRI photometry. We report in this paper the results of these observations.

2. Observations

2.1. Spectroscopy

Low resolution spectra of LM have been obtained with the 1.22m telescope operated in Asiago by the University of Padova. A Boller & Chivens spectrograph is attached to the Cassegrain focus feeding light to an ANDOR iDus DU440A camera, that houses a back-illuminated E2V 42-100 CCD (2048 X 512 array, $13.5\ \mu\text{m}$ pixel). A $300\ \text{ln mm}^{-1}$ grating blazed at $5000\ \text{\AA}$ was adopted, allowing to cover the $3300\text{--}8000\ \text{\AA}$ range at $2.31\ \text{\AA}/\text{pix}$ dispersion. Data reduction was carried out in IRAF and involved the usual steps on bias and dark removal, flat-fielding, variance-weighted spectrum tracing, sky subtraction, wavelength calibration via FeHeAr lamp, heliocentric correction and flux calibration (via observations of the nearby spectrophotometric standard HR 7867). LM has been observed twice on Dec 6 and 14, 2019, exposing for 16min on both occasions. The spectra look identical and their average is plotted in Figure 1. A comparison is there provided with HD 188512, a template for the G8 IV spectral class according to Yamashita et al. (1977), observed with exactly the same telescope setup as for LM, and selected from the Asiago Spectral Database (U. Munari, in preparation).

2.2. Photometry

Optical photometry of LM in the Landolt (1992) photometric system has been obtained with a Richey-Chretien 0.4m f/8 telescope located in Monte Baldo (Verona, Italy), equipped with a Moravian G4 CCD camera ($36\times 36\text{mm}$ active area, $12\ \mu\text{m}$ size) and B,V,R,I photometric filters from Astrodon. The B filter is of the new version, corrected for the red-leak of its original version (see Munari and Moretti 2012). The photometry of LM that we have collected in five distinct nights is presented in Table 1.

Data reduction has involved all the usual steps for bias, dark, flat with calibration images collected during the same observing nights. We adopted aperture

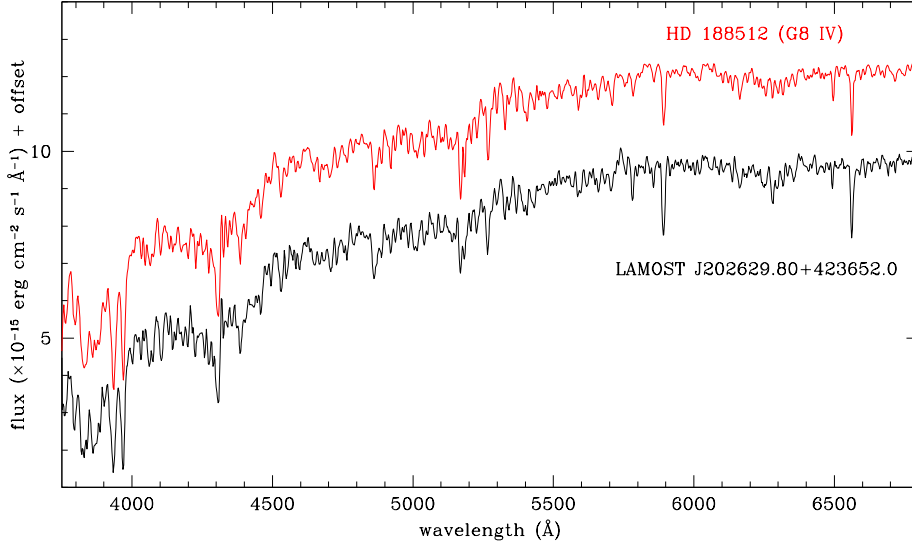


Figure 1. Our spectrum of LAMOST J202629.80+423652.0 compared to that of HD 188512 (+offset), template for the G8IV spectral type.

photometry because the sparse field around LM did not required PSF-fitting procedures. The transformation from the local to the Landolt standard system was carried out via color equations calibrated on a photometric sequence recorded on the same frames as LM:

$$\begin{aligned}
 V &= v + \alpha_v \times (v - i) + \gamma_v \\
 B - V &= \beta_{bv} \times (b - v) + \delta_{bv} \\
 V - R &= \beta_{vr} \times (v - r) + \delta_{vr} \\
 V - I &= \beta_{vi} \times (v - i) + \delta_{vi}
 \end{aligned}$$

The local photometric sequence has been extracted from APASS DR8 survey (Henden and Munari 2014), ported to the Landolt system via the transformations calibrated by Munari et al. (2014). The errors quoted in Table 1 are the quadratic sum of the Poissonian and the transformation contributions.

3. Results

3.1. A normal spectral appearance

The spectrum of LM presented in Figure 1 is that of a normal, sub-giant star of the G8IV spectral type, abundant in the Solar Neighborhood as indicated by Gaia DR2 stellar census (Gaia Collaboration 2018). No Mira is known to

Table 1. Our BVRI photometry (on the Landolt system of equatorial standards) of LAMOST J202629.80+423652.0.

obs. date	B	V	R	I
2019-12-07.8957		14.439 ± 0.009	13.766 ± 0.010	13.041 ± 0.014
2019-12-14.8155		14.456 ± 0.006	13.773 ± 0.007	13.119 ± 0.016
2020-01-08.8245	15.629 ± 0.032	14.454 ± 0.011	13.760 ± 0.010	13.100 ± 0.015
2020-01-09.8242	15.603 ± 0.061	14.478 ± 0.029	13.737 ± 0.017	13.076 ± 0.025
2020-01-16.7712	15.580 ± 0.019	14.454 ± 0.006		
weighted mean	15.610 ± 0.020	14.463 ± 0.004	13.755 ± 0.005	13.084 ± 0.008

have such an early spectral type (cf. VSX database¹). In our spectrum of LM no emission line is visible.

Li et al. (2015) report the presence of strong $H\alpha$, $H\beta$ and [OIII] emission lines in their spectrum of LM. They come actually from the sky-background emission originating from the huge HII region IC 1318 associated to nearby γ Cyg (10° angular extent). In Figure 2 we present the sky-background at 15arcsec away from LM as recorded on our spectrum. It looks identical to the spectrum attributed to LM by Li et al. (2015).

Li et al. (2015) also report about the detection in their spectrum of LM of Raman scattered OVI lines at 6830 and 7088 Å (Schmid 1989). These are actually normal OH lines forming in the Earth's atmosphere, frequently used for wavelength calibration of high resolution spectra at far-red wavelengths (cf. Osterbrock et al. 1996). In Figure 3 we plot the far-red portion of the sky-background at 15arcsec distance from LM taken from our spectrum of the program star, with superimposed the identification of Meinel rotation-vibration bands of OH.

We therefore conclude this section noting that nothing in the spectrum of LM supports a classification as a SySt: all lines and features seen in emission by Li et al. (2015) seems actually due to inaccurate handling of sky-background subtractions.

3.2. No photometric variability

Li et al. (2015) also classified LM as a pulsating Mira. Our photometry in Table 1 extends over too short a time interval to draw any conclusion about a possible variability affecting LM. To investigate the matter further, we retrieved the patrol photometry of LM collected by ASASSN (Shappee et al. 2014, Kochanek et al. 2017) and ZTF all-sky patrol surveys (Masci et al. 2019, Bellm et al. 2019). The ASASSN and ZTF photometry in the g' , r' , and V bands is plotted in Figure 4. It extends from 2015 to 2019. No variability is present in excess of the

¹<https://www.aavso.org/vsx/>

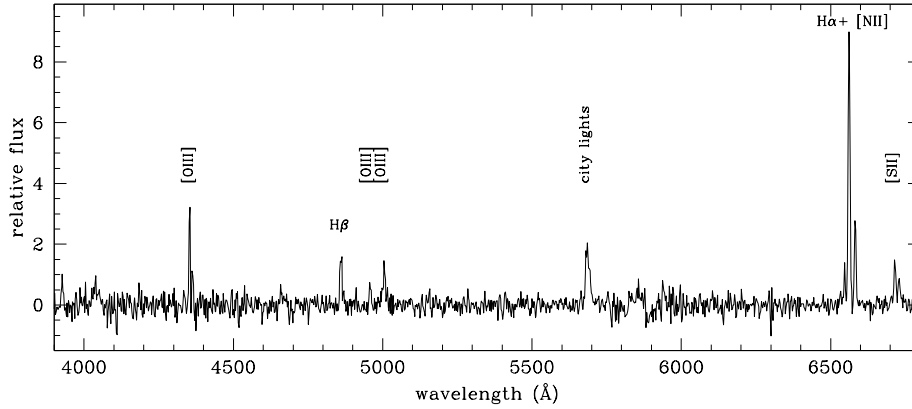


Figure 2. Emission lines from the sky-background around LAMOST J202629.80+423652.0 in our spectrum, due to diffuse emission from the HII region around γ Cyg.

observational noise, and this precludes the classification reported by Li et al. (2015) of LM as a Mira.

3.3. No circumstellar dust

Li et al. (2015) attributed a D-type classification to LM, i.e. the presence of warm dust around it. As illustrated by Allen (1982) the excess emission from such warm dust (500–1000 K) is already evident in the H band ($1.6 \mu\text{m}$) and become prominent in the K band ($2.2 \mu\text{m}$). To investigate the spectral energy distribution (SED) of LM, we take advantage of the absence of photometric variability (established in the previous section) that allows to combine non-simultaneous data gathered by different surveys over the whole wavelength range. The SED for LM built from our BVRI observations (Table 1), 2MASS JHK_s and AllWISE W₁W₂W₃ data is presented in Figure 5, together with the reference SED for a typical G8 IV field star using colors from Fitzgerald (1970), Cousins (1976), and Koornneef et al. (1983). The two become a fine match once a correction for $E_{B-V}=0.35$ reddening is applied to LM. In conclusion, the SEDs in Figure 5 excludes the presence in LM of any dust hotter than ~ 100 K (constrain set by W₃).

3.4. Fundamental parameters

The GAIA second release (GAIA-DR2) lists a parallax $\pi = 0.761 \pm 0.018$ (mas) for LM. The fractional error is less than 20% and therefore is straightforward to derive the distance to LM as $d=1.31$ kpc by direct inversion of the Gaia parallax. At such a distance along the line of sight to LM, the Bayestar 3D Galactic

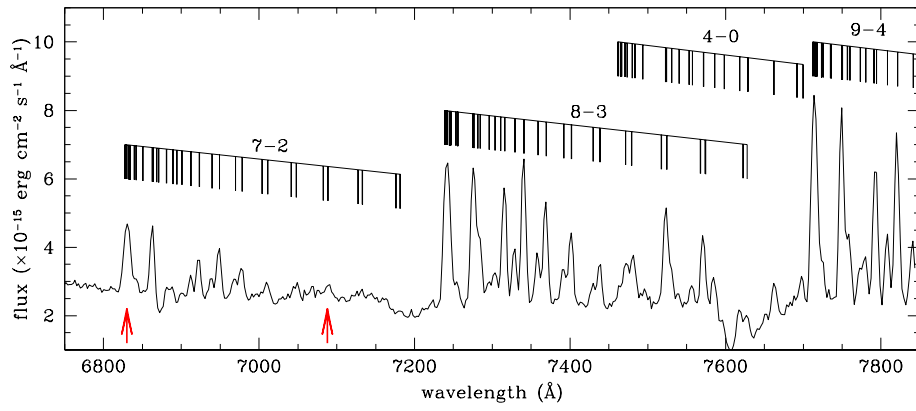


Figure 3. Emission in the far-red of the sky-background around LAMOST J202629.80+423652.0 in our spectrum, highlighting the Earth's OH emission (with Meinel rotation-vibration bands identified). The red arrows points to telluric OH lines labelled by Li et al. (2015) as due to Raman scattered OVI 6825, 7088 Å.

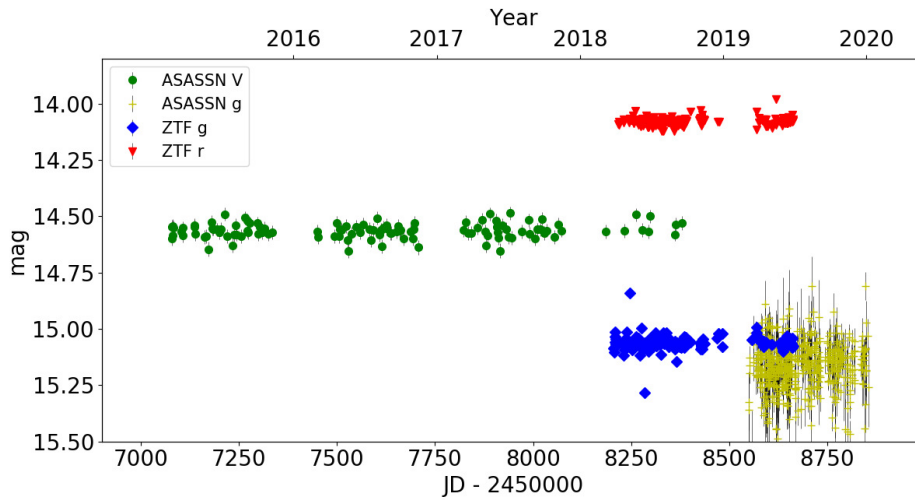


Figure 4. Photometric data of LAMOST J202629.80+423652.0 obtained by ASAS-SN and ZTF sky patrol surveys.

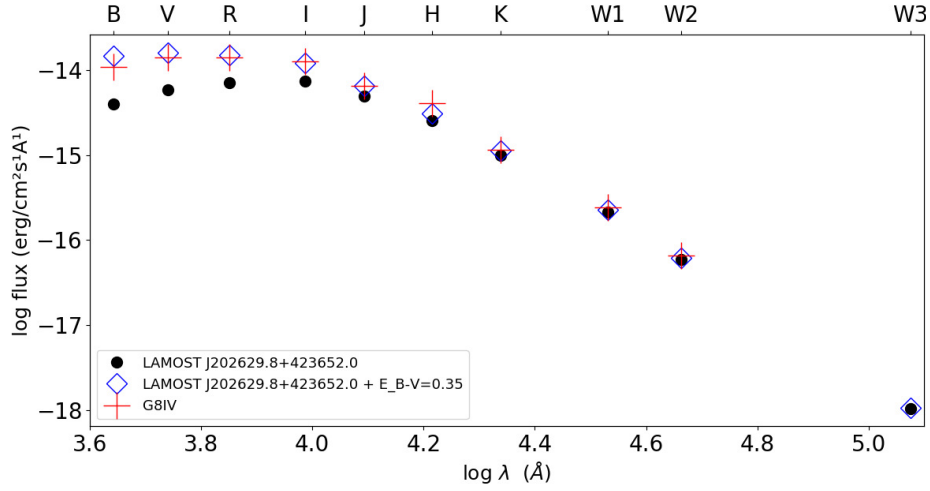


Figure 5. Spectral energy distribution of LAMOST J202629.80+423652.0 as observed (black dots), and after correction for $E_{B-V}=0.35$ reddening (blue diamonds). The red crosses illustrate the intrinsic energy distribution of a G8 IV star from tabular data.

extinction map (Green et al. 2019) lists a reddening of $E(g-r) = 0.41$, that transforms to $E(B-V)_0 = 0.35$ for a standard $R_V = 3.1$ interstellar reddening law following the relations for G-type stars by Fiorucci and Munari (2003). This is in excellent agreement with the value of the reddening necessary to bring the SED of LM in agreement with that of a typical G8 IV star in Figure 5. With such a reddening and distance, the mean V -mag value in Table 1 transforms to an absolute magnitude for LM of $M(V)=2.78$. This is in fine agreement with the absolute magnitudes reported by Sowell et al. (2007) that list $M(V)=5.50$, 3.20 and 1.35 for G8 stars of luminosity class V, IV and III, respectively. According to tabular values in Straižys (1992), such a star is characterized by a temperature of 5100 K, a luminosity of $4.4 L_\odot$ and a radius of $2.7 R_\odot$.

4. Conclusions

We have obtained new photometric and spectroscopic observations of LAMOST J202629.80+423652.0 that combined with literature data shows it to be a normal G8 IV sub-giant star, and not a symbiotic star. Such a classification by Li et al. (2015) appears due to inaccurate sky-background subtraction to their spectra.

References

- Akras, S., Guzman-Ramirez, L., Leal-Ferreira, M.L., Ramos-Larios, G., A census of symbiotic stars in the 2MASS, WISE, and GAIA survey, 2019, *Astrophys. J., Suppl. Ser.*, **240**, p.21, DOI: 10.3847/1538-4365/aaf88c

- Allen, D.A., The Nature of Symbiotic Stars, 2000, ed. M. Friedjung and R. Viotti, IAU Colloq, 1982, **95**, 20 + 310 p
- Belczyński, K., Mikoajewska, J., Munari, U., Ivison, R., Friedjung, M., A catalogue of symbiotic stars, 2000, *Astron. Astrophys., Suppl.*, **146**, p.407, DOI: 10.1051/aas:2000280
- Bellm, E.C., et al., The Zwicky Transient Facility: System Overview, Performance, and First Results, 2019, *Publ. Astron. Soc. Pac.*, **131**, p.018002, DOI: 10.1088/1538-3873/aacbe
- Cousins, K.W.J., VRI standards in the E regions, 1976, *Mem. Royal Astron. Soc.*, **81**, p.25
- Fiorucci, M., Munari, U., The Asiago Database on Photometric Systems (ADPS). II. Band and reddening parameters, 2003, *Astron. Astrophys.*, **401**, p.781, DOI: 10.1051/0004-6361:20030075
- Fitzgerald, M. Pim., The Intrinsic Colours of Stars and Two-Colour Reddening Lines, 1970, *Astron. Astrophys.*, **4**, p.234
- Gaia Collaboration., Mignard, F., Klioner, S.A., Lindegren, L., Hernandez, J., Bastian, U., Bombrun, A., Hobbs, D., Lammers, U., Michalik, D., Ramos-Lerate, M., Biermann, M., Fernandez-Hernandez, J., Geyer, R., Hilger, T., Siddiqui, H.I., Babusiaux, C., Barache, C., Lambert, S., and more., Gaia Data Release 2. The celestial reference frame, 2018, *Astron. Astrophys.*, **616**, p.A14, DOI: 10.1051/0004-6361/201832916
- Green, Gregory M., Schlafly, Edward., Zucker, Catherine., Speagle, Joshua S., Finkbeiner, Douglas., A 3D Dust Map Based on Gaia, Pan-STARRS 1, and 2MASS, 2019, *Astrophys. J.*, **881**, p.93, DOI: 10.3847/1538-4357/ab5362
- Henden, A., Munari, U., The APASS all-sky, multi-epoch BVgri photometric survey, 2014, *Contrib. Astron. Obs. Skalnaté Pleso.*, **43**, p.518
- Kochanek, C.S., Shappee, B.J., Stanek, K.Z., Holoiien, T.W.-S., Thompson, Todd A., Prieto, J.L., Dong, Subo, Shields, J.V., Will, D., Britt, C., Perzanowski, D., Pojmaski, G., The All-Sky Automated Survey for Supernovae (ASAS-SN) Light Curve Server v1.0, 2017, *Publ. Astron. Soc. Pac.*, **129**, p.104502, DOI: 10.1088/1538-3873/aa80d9
- Koornneef, J., Near-infrared photometry. II. Intrinsic colours and the absolute calibration from one to five micron, 1983, *Astron. Astrophys.*, **500**, p.247
- Landolt, Arlo U., UBVRI Photometric Standard Stars in the Magnitude Range 11.5 $\leq V \leq 16.0$ Around the Celestial Equator, 1992, *Astron. J.*, **104**, p.340, DOI: 10.1086/116242
- Li, Jiao., Mikolajewska, Joanna., Chen, Xue-Fei., Luo, A. -Li., Rebassa-Mansergas, Alberto., Hou, Yong-Hui., Wang, Yue-Fei., Wu, Yue., Yang, Ming., Zhang, Yong., Han, Zhan-Wen., The first symbiotic stars from the LAMOST survey, 2015, *RAA.*, **15**, p.1332, DOI: 10.1088/1674-4527/15/8/016

- Masci, F. J. et al., The Zwicky Transient Facility: Data Processing, Products, and Archive, 2019, Publ. Astron. Soc. Pac., **131**, p.018003, DOI: 10.1088/1538-3873/aae8ac
- Mukai, K. et al., SU Lynxis, a hard X-ray bright M giant: clues point to a large hidden population of symbiotic stars, 2016, Mon. Not. R. Astron. Soc., **461**, p.L1, DOI: 10.1093/mnrasl/slw087
- Munari, U., in The Impact of Binary Stars on Stellar Evolution, G. Beccari and H.M.J. Boffin eds, 2019, Cambridge Univ. Press., p.77, arXiv:190901389, DOI: 10.1017/9781108553070
- Munari, U., Moretti, S., Characterizing the Photometric Response of the ANS Collaboration Monitoring Program, 2012, Baltic Astronomy., **21** p.22, DOI: 10.1515/astro-2017-0354
- Munari, U., Henden, A., Frigo, A., APASS discovery and characterization of 180 variable stars in Aquarius, 2014, JAD., **20**, p.4
- Osterbrock, D.E., Fulbright, J.P., Martel, A.R., Keane, M.J., Trager, S.C., Basri, G., Night-Sky High-Resolution Spectral Atlas of OH and O2 Emission Lines for Echelle Spectrograph Wavelength Calibration, 1996, Publ. Astron. Soc. Pac., **108**, p.277
- Sowell, J. R., et al., H-R Diagrams Based on the HD Stars in the Michigan Spectral Catalogue and the Hipparcos Catalog, Astron. J., 2007, **134**, p.1089, DOI: 10.1086/520060
- Schmid, H.M., Identification of the emission bands at 6830, 7088 Å, 1989, Astron. Astrophys., **211**, p.L31
- Shappee, B.J., Prieto, J.L., Grupe, D., Kochanek, C.S., Stanek, K.Z., De Rosa, G., Mathur, S., Zu, Y., Peterson, B.M., Pogge, R.W., Komossa, S., Im, M., Jencson, J., Holoiien, T.W.-S., Basu, U., Beacom, J.F., Szczygie, D.M., Brimacombe, J., Adams, S., Campillay, A., et al., The Man behind the Curtain: X-Rays Drive the UV through NIR Variability in the 2013 Active Galactic Nucleus Outburst in NGC 2617, 2014, The Astronomical Journal., **788**, p.48, DOI: 10.1088/0004-637X/788/1/48
- Straižys, V., Multicolor stellar photometry, 1992, Tucson : Pachart Pub. House, c1992
- Yamashita, Y., Nariai, K., An Atlas of representative stellar spectra, 1977, University of Tokio Press

Formation of magnetized spatial structures in the Beta Lyrae system

I. Observation as a research background of this phenomenon

M. Yu. Skulsky

Lviv Polytechnic National University, Department of Physics, 79013, Lviv, Ukraine, (E-mail: mysky@polynet.lviv.ua)

Received: February 27, 2020; Accepted: April 3, 2020

Abstract. The discovery of the donor magnetic field has repeatedly posed the task of a thorough study of the phenomenon, which is based on the concept of the influence of the magnetic field on the processes of the formation of gaseous structures and mass transfer in the Beta Lyrae system. This article provides an overview, analysis, and synthesis of the results of a variety of long-term observations as a necessary basis for further clarification of issues aimed primarily at the study of magnetized gaseous structures. As part of such a study, it was found that the structure of the gaseous flows between the donor and the gainer varies in some way depending on the phases of the orbital period; and, accordingly, that the donor magnetic field influences the formation of these moving magnetized structures. The analysis of the masses of both components for use in further scientific works suggests that the following values are optimal: $2.9 M_{\odot}$ for the donor and $13 M_{\odot}$ for the gainer. The study of satellite lines leads to the fact that the accretion disk surrounding the gainer consists of two parts: the external satellite disk and the internal massive opaque disk. From the analysis of all observations and studies of the magnetic field, observations on the 6-m telescope can be considered the most reliable. They have formed the spatial configuration of the donor magnetic field, which is important for studying and understanding the features of the mass transfer in this interacting system. Further evidence regarding the picture of the magnetized accretion structures as the special phenomenon will be presented in the forthcoming articles.

Key words: binaries: individual: Beta Lyrae – emission-line: magnetic field: mass-transfer

1. Introduction

Our spectral and spectrophotometric observations of the known interacting binary Beta Lyrae were conducted in 1965-2010 on different telescopes, in particular, on the 6-m and 2.6-m telescopes at the Special and Crimean Astrophysical

Observatories using CCD detectors and polarization analyzers. The most important results are the first definition of the masses of both components directly from the complex spectra of the binary system (Skulskij, 1975b, 1992), simultaneously with the discovery and research of the donors magnetic field (Skulskij, 1985; Skulskij & Plachinda, 1993), as well as the study of the structure of the accretion disk surrounding the gainer (Skulskij, 1993a,c,b). The results of the last two directions of our observations and researches are outlined in various editions forming certain ideas about the basic physical properties of the Beta Lyrae system, which is in the phase of the rapid mass transfer. But, they are practically not used in another, methodologically dissimilar, studies in interpreting its nature. This applies, e.g., the articles of Mennickent & Djurašević (2013) and Mourard et al. (2018), where the progress in the modelling of light curves of the Beta Lyrae system was made, in particular, the significant contribution of the radiation of the accretion disk to the light curves was established.

In this sense, the identification of two hot regions (or spots) on the accretion disk in Mennickent & Djurašević (2013) was of particular interest. These regions are observed in the phases of 0.80 P and 0.40 P and their temperatures are 10% and 20% higher than the average on the disk. The authors supposed that these hotter regions illuminated by the donor may be formed by the collision of gas flows with the disk during mass transfer between the components of this system (but without any mechanism suggested for both hot regions). At the same time, the results of this light curve modeling can be interpreted in the light of studies of the accretion disk properties at the presence of the donor magnetic field. Indeed, the hotter region of the accretion disk at the phase 0.40 P of the first quadrature is naturally explained by the deflection by the Coriolis force of the main gas flow that is directed from the donor through a Lagrange point to the gainer's Roche cavity and with a further collision of this flow with the accretion disk. This hotter region and its location are well known. In particular, it was clearly detected by Burnashev & Skulskij (1991) absolute spectrophotometry of the Beta Lyrae system and followed from various spectropolarimetric observations. However, such a classical hydrodynamic picture cannot be suitable for explaining of the heated part of the accretion disk in the orbital phases near 0.80P of the second quadrature. Here, this should be based on another understanding of the sources of this disk heating and the structure of the accretion flows between the components of this interacting binary system, given the presence and influence of the donor magnetic field. Such understanding was formed mainly in a number of original observations and investigations in 1980–1995.

In this situation, there was a need for a consistent generalized statement of certain aspects of our spectral studies based on the concept of the reality of magnetized gaseous structures that reflect the specific configuration of the donor magnetic field. The photometry and absolute spectrophotometry data, orbital variability of donor magnetic field curves, radial velocities and intensities of complex lines in different spectral regions, etc. were analyzed. As a first result, the preliminary data to a pattern of the accretion flows was briefly represented

by Skulsky (2015, 2018). However, due to a large increase in data in the study of diverse observations, this summarized research had to be divided into three related articles. The purpose of this article is to give a brief description of both our spectral observations and other diverse studies as a prerequisite for creating a general mass transfer picture in the presence of the donor magnetic field.

2. Introductory description of properties and a schematic picture of the Beta Lyrae system

Preliminary data from this large study suggest that a further generalized description and investigation of the physical properties of the Beta Lyrae system will be better comprehensible after giving a brief description of the verified facts and some illustration.

According to the absolute spectrophotometry by Burnashev & Skulskij (1978) and spectral observations by Skulskij (1992, 1993b), one can assume (see Fig. 1) that the interacting system Beta Lyrae in the range of $\lambda\lambda$ 3400 – 7300 Å contains the bright donor of type B8III of mass $2.9 M_{\odot}$, the massive gainer of mass $13 M_{\odot}$ masked by an opaque thick accretion disk with a pseudophotosphere of A5III type, and the hydrogen envelope with temperature close to $T_e = 20000K$. The chemical composition of the atmosphere of the donor is peculiar and undergoing hydrogen burning in the CNO cycle (Skulskij, 1975a, 1986; Balachandran et al., 1986). It is believed that the donor practically fills up its Roche cavity and is in the final stage of mass loss and transfer, the rate of which is close to $2 \cdot 10^{-5} M_{\odot}/yr$. As Umana (2002) noted, the radio emission from the binary system supports the presence of an extra source of continuum emission generated by stellar winds with a mass loss rate of $5 \cdot 10^{-7} M_{\odot}/yr$. In this binary system, there are well-developed circumstellar structures, in particular, of the accretion disk surrounding the gainer. This disk is formed by at least two components (Skulskij, 1992, 1993b): an outer translucent, so-called satellite disk, whose rotational effect is clearly apparent in its projection on the donor at the phases only before and after the donor eclipse, and an optically thick opaque massive disk (approximately of $(10^{-4} - 10^{-3}) M_{\odot}$ by Mourand et al., 2018). After measurements of hundreds of Zeeman spectrograms, magnetic field was detected in the donor atmosphere, which quasi-sinusoidally changes over of orbital period phases (Skulskij, 1982, 1985). The dipole magnetic field with an axis directed in the direction of orbital phases of (0.355-0.855) P has the maximum on the donor surface at the 0.855 P phase, reflecting the location of this magnetic pole facing the gainer. This means that the ionized gas, channeled by the donor magnetic field, can move in the direction of its dipole axis from the donor surface and deflects along the magnetic field lines toward the accretion disk (Skulsky, 2015, 2018). The correlation between the phase variability in the absolute flux in the H emission line and that in the effective magnetic field of the donor was discovered Burnashev & Skulskij (1991). This was the first substantial fact to

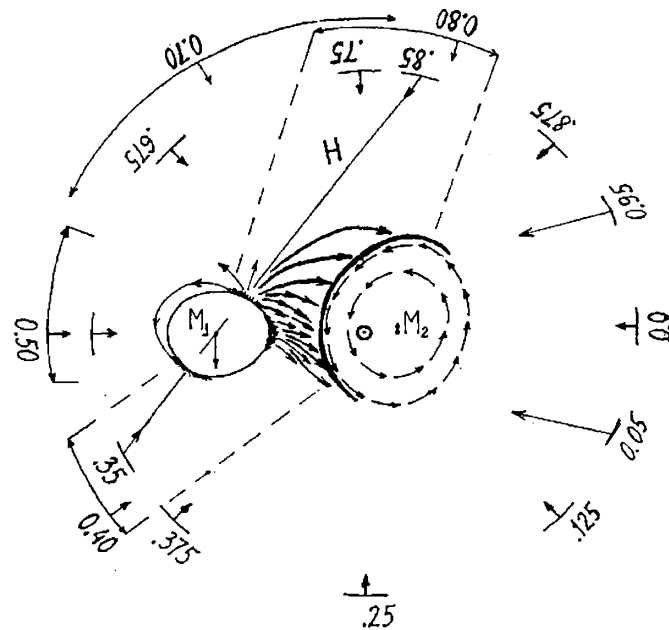


Figure 1. A schematic model of the Beta Lyrae system (top view on the orbital plane). It contains the bright donor (reaches its Roche lobe) of mass $2.9M_{\odot}$ and the gainer of mass $13M_{\odot}$ masked by an opaque accretion disk. The distance between the centers of the two components on the real scale is $58R_{\odot}$ (small circle shows the gravity center of the binary system). More important phases (as fractions of the orbital period), the directions of the orbital motion of two components, and the dipole axis of the donor effective magnetic field (denoted by "H") are shown by straight arrows. The fan-shaped gaseous accretion flows, represented by curved arrows, form a hot arc (bold line) on the outer rim of the accretion disk facing the donor. The dimensions of the outer part of the accretion disk (so-called satellite-disk) are represented by two rows of round arrows in the direction of its rotation. This rotation in the direction towards and from the observer is shown, respectively, in phases $0.05P$ and $0.95P$ (phase $0.0P$ corresponds to the center of the primary eclipse). Two hotter regions on the disk, proposed at the modeling of light curves by Mennickent & Djurašević (2013), are marked in the phases of $0.40P$ and $0.80P$ by dashed limits directed at the centers of both components.

support the concept that the magnetic field has a significant effect on the spatial formation of gaseous structures during mass transfer in the Beta Lyrae system. This fact was confirmed by the results of further observations. It is hoped, that a better understanding of the basic research in this article will be facilitated by the presentation in Figure 1 of a schematic model of this binary system.

3. Results of the most significant observations and investigations of the Beta Lyrae system

This article is not intended to be a detailed review of all Beta Lyrae publications, a full description can be found in Sahade (1980). Recent observations, especially regarding the topic of modern modeling of light curves, were reported, for example, in Mourard et al. (2018). The following sections will give a more detailed overview of the important observations, the results of their research and the interpretation that are related to the coverage of the declared topic. To illustrate some observed facts, we will sometimes use original drawings from the articles cited.

3.1. Photometry of the Beta Lyrae system and simulations of its light curves

Numerous photometric publications about the Beta Lyrae system affirm constant interest in its physical nature. Starting from the observations of Goodricke & Englefield (1785), the orbital period increased by 0.05 d and now is reaching 12.94 d. This clearly indicates the phase of rapid mass transfer between both components. It is characterized by a high rate of about $2 \cdot 10^{-5} M_{\odot}/yr$, whereas the age of this massive interacting system of near $2.5 \cdot 10^{-7}$ years is relatively young. As a result, well-developed gaseous structures are observed in this binary system (a certain presentation of there is given in Fig. 1). That is why the main focus in modern modeling of light curves of the Beta Lyrae system is paid to the radiation of the circumstellar structures, especially the accretion disk, and their physical properties.

The well-known “light curve of type Beta Lyrae” in modern observations, presented in Fig. 2, was published by Harmanec et al. (1996). Their data set is often used in light curve simulations based on the idea of an optically thick accretion disk surrounding the massive gainer.

According to a number of light curve simulations, including recent studies Mennickent & Djurašević (2013) and Mourard et al. (2018), it can be considered that this opaque disk starts from the gainer with its radius of $6 R_{\odot}$ at the semi thickness of the disk that is about $6.5 R_{\odot}$, the radius of the outer rim reaches $30 R_{\odot}$, and the binary orbital inclination ranges from 81° to 93.5° . The authors indicate a significant contribution of the radiation of this disk to the total light curve from the side of the disk facing the donor. Although the idea of heating this part of the disk, including interaction with the falling gas flows, is considered in many models, there are new aspects. The radial temperature profile of the disk varies from 30000 K to 8000 K, where the central regions of the disk are heated by the embedded gainer. On outer edges of this disk their surface temperatures are essentially different, particularly from the side of the disk facing the donor where there is a wide asymmetric hotter region with the temperature that can reach 10000 K. The light-curve model of Mennickent & Djurašević (2013) has

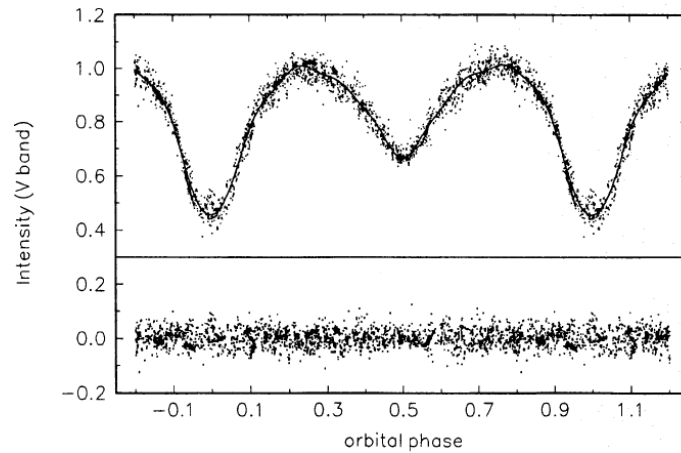


Figure 2. The V-band light curve (λ 5500 Å) (Harmanec et al., 1996).

shown two hotter regions in the phases 0.80 P and 0.40 P, covering respectively 30% and 10% of the accretion disk edge. Their temperatures are higher by 10% and 20% from the mean value on the disk edge. The wide bright region in the phase 0.80 P concerns of the second quadrature, in which the accretion disk contributes 22% to the total V-band light curve (that is matched with the Beta Lyrae absolute spectrophotometry of Burnashev & Skulskij (1978)).

Examining a question of the different geometric shapes of the accretion disk, Mourard et al. (2018) made considerable progress in the simulations of the light curves from the far ultraviolet to the infrared region. However, there are some difficulties in harmonizing the results of the modeling of light curves relating to the bands where the crossover is observed at depths of minima (see, for example, the band curves at 1250 Å and 1365 Å in Kondo et al. (1994)). This is especially true of the spectral region at wavelengths shorter than the Lyman limit, where, according to Kondo et al. (1994), the band curves at 965 Å and 1085 Å show that the Beta Lyrae system here looks not at all as an eclipsing binary. These Voyager satellite observations have shown that light curves outside the Lyman limit are deformed in such a way that they lose their characteristic features that are typical for the visible spectrum shown in Fig. 2. The ultraviolet light curve at 1085 Å (see Fig 3, which is borrowed from Kondo et al. (1994)) becomes almost flat with a clear maximum of the radiation in the second quadrature. Such a light curve at 965 Å in the same second quadrature looks as quasi-sinusoidal, with the observed outburst lasting several days. Hence, that in the (0.6-0.8) P phases of the second quadrature (see Fig. 1), to the left of the direction (0.5-1.0) P, the dominant region of shock collision of the hot turbulent plasma with the accretion disk is observed, reflecting the spatial configuration of the donor magnetic field (Skulskij, 1985).

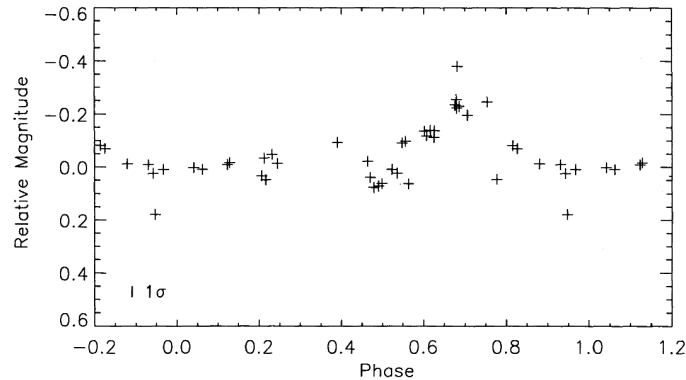


Figure 3. The ultraviolet light curve (λ 1085 Å) (Kondo et al., 1994).

Understanding the nature of the Beta Lyrae system based on the light curve solutions requires taking into account all available data. An important factor is the existence of the soft X-ray emission (below 10 keV), which does not change with the phase of the orbital period and is not obscured by both components. According to Ignace et al. (2008), this soft X-ray emission must radiate over the orbital plane, probably due to the Thomson scattering of X-rays in the stellar wind of the hot gainer, or this may be due to shock collision gaseous flows with the accretion disk. This approach is supported by the observation of the radio-nebula, surrounding the Beta Lyrae system up to 40 AU, which indicates the substantial non-conservative mass-loss during the evolution of this interacting system (Umana et al., 2000).

3.2. The 283 d photometric periodicity and the coherent system of secondary periods

The question of the reality of secondary non-orbital periods in the Beta Lyrae system and the nature of the corresponding periodic processes are discussed over a hundred years. The ranges of changes of periodicities and resonances of physical parameters are observed from tens of seconds to tens of years. Particular attention deserves non-orbital of 283 d photometric periodicities established quite reliably in two consecutive articles. Its first value of (283.39 ± 0.26) d was obtained by Van Hamme et al. (1995) based on the deviations from the averaged light curves for the past 150 years of the Beta Lyrae observations that are centered at about 1920. A year later, this period was determined by Harmanec et al. (1996) with even greater accuracy (282.405 ± 0.070) d, based on the averaged V-curve. It consists of 2582 V-band magnitudes obtained in a 36 yr period up to 1989 and is presented in Fig. 2. At the same time, investigating the variability of the emission lines of Harmanec et al. (1996), the secondary period of 4.478 d

was found. It turned out that this short period, the orbital period, and the period 282.425 d are related by a simple equation. In addition, Peel (1997) showed that in periodograms based on observations between 1898 and 1916, the peaks of periods of 283 d and 340 d are clearly visible, with a significantly stronger peak of 340 d. Burnashev & Skulskij (1980), based on the narrowband absolute spectrophotometry of Beta Lyrae in 1978-1979, derived quasiperiodic variations of the radiation flux in H_α -line emission being 1/7 of the orbital period.

The increase of the orbital period owing to the rapid mass transfer from the donor to the gainer logically results in the idea of coordinated variability in time of all known secondary periods. This topic was considered by Skulsky (2000) in view of all aspects of a question on the donor as a magnetic rotator. There was presented a coherent system of periodicities that included already known periods, with new periods of 10.93 d, 13.23 d, and 564.85 d. In particular, the difference of 0.965 d between the values of a long period in the articles of Van Hamme et al. (1995) and Harmanec et al. (1996) was simply explained by two different sets of observational data, the effective centers of which were shifted in time by about 60 years. It turned out that studies of all secondary periods should be carried out in conjunction with the research of the magnetic field and the spatial structure of the accretion disk (Skulsky, 2000, 2007). And this created the prerequisites for the detection of a coherent system of secondary periods and resonances, which changes synchronously with the increase of the orbital period. It has been established that the long period of 283 d can be a proof of the synchronization between the precession rotation of the outer part of the accretion disk (i.e., of a satellite-disk, see Fig. 1) and the tidal wave on the surface of the donor. The 283 d, 340 d, and 565 d periods may reflect variable substructures of outer layers of the accretion disk, whose dynamic parameters are related to each other as integers.

3.3. Phenomenon of the satellite lines and physical properties of the accretion disk

The original feature of the absorption spectrum of the Beta Lyrae system, unusual for interacting systems of the W Ser type, is the so-called satellites of absorption lines. They appear near some absorption lines in the binary system spectrum in the phases of 0.1-0.9 P of the main eclipse, disappearing within 0.02 P in the center donor eclipse. The system of satellite lines changes a sign of their radial velocities to the opposite at the passage of the main eclipse. It is believed that the satellite lines are formed in the gas substance of the outer edges of the accretion disk when it passes in front of the bright donor. In our long investigations of the Beta Lyrae spectrum and based on well-known studies starting with Struve (1941), we proceeded from the interpretation of satellite lines based on the idea of the rotation effect of the outer layers of the accretion disk. Finally, there was a need for more purposeful research of the satellite lines system as a key to understanding the structure of the accretion disk. Therefore,

in 1985-1992 such research became a priority as observations were carried out with high spectral resolution and a signal-to-noise ratio on the 2.6-m CrAO telescope using a CCD detector. The phenomenon of the origin, development, and disappearance of the satellite lines HeI, H, MgII and SiII in the phases of the main eclipse was studied on the basis of measuring their radial velocities and equivalent widths. Also, in these years, one conducted a comprehensive study of the lines of the donor and gainer and the emission in the SiII $\lambda\lambda$ 6347, 6371 doublet. The main results of our first study, published in Skulskij (1992), are as follows.

The movement of satellite lines in the Beta Lyrae spectrum indicates the spatial stratification of their formation in the accretion disk. The radial velocity curves of satellite lines belonging to different chemical elements differ by their amplitude and other characteristics due to the difference between excitation and ionization potentials. These curves are asymmetric relative to the main eclipse median. The helium satellite lines have the greatest amplitude of change (from +240 km/s in the phase 0.96 P before the eclipse center to -290 km/s in the 0.02 P phase after the eclipse center). The satellite lines of silicon show considerable change, correspondingly from +215 to -280 km/s, while the magnesium lines show, respectively, even smaller changes from +205 to -250 km/s. Taking into account the velocity of the center of mass of the binary system of -18 km/s one can say that the negative velocities in the disk after the center of the eclipse are slightly higher than their positive velocities before the eclipse center. This indicates the phase asymmetry of the dynamic characteristics of the satellite lines: the maxima of the radial velocity curves are within phases of (0.035-0.045) P, phases before the eclipse center (i.e., in the phase of 0.96 P) and within phases of (0.01-0.02 P) after this center. In the phases closest to the eclipse center (and to the center of the disk) one sees the maximum of the radial velocity curve for the helium satellites that indicates the higher temperatures of the medium of their formation. The phase dependence of the equivalent width of the satellite lines indicates the limits of their occurrence and disappearance in the phases up to (0.89 P and 0.98 P) and after (0.01 P and 0.11 P) the eclipse center, as well as the respective phases of their maximum intensity at (0.95 P and 0.05 P). The satellite lines disappear and reappear asymmetrically relative to the median of the eclipse at complete absence in the spectrum in the range greater than 0.02 P, indicating the boundaries of the internal asymmetric opaque disk.

The revealed patterns of satellite lines are shown in Fig. 4 and schematically reflected in Fig. 1 in the model of a satellite-disk, which has an elongated oval shape in the direction of the gainer's movement. The ratio of the axes of this disk is about 4/3. The greater half of the long axis shows some stratification for the disk layers with different chemical elements in the range of about 0.1 of the distance between the centers of the two components. On the backside of the gainer, where the radius of the disk is smaller, the rotating speed of its outer edges is higher. This is probably due to the action of the main gas stream that pushes here the outer part disk up to the surface of the gainer. Stratification of

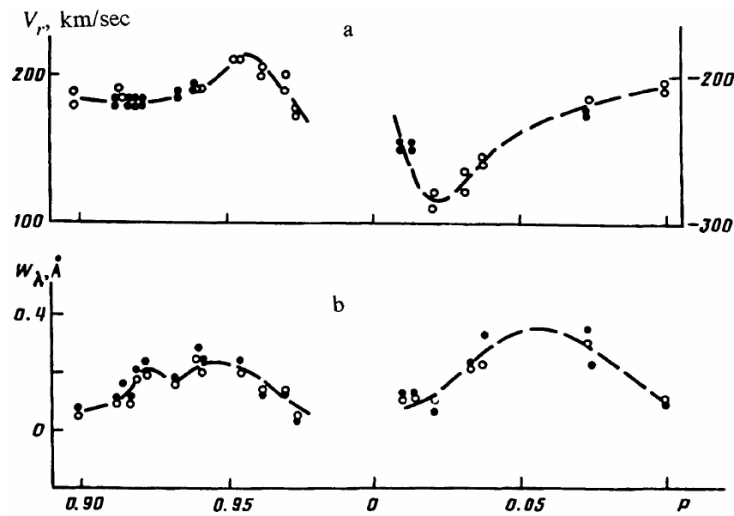


Figure 4. a) Radial velocity curves of silicon line satellites, according to observations in 1991 (light circles) and 1992 (dark circles) (V_r -scales in phases before and after the eclipse center are vertically offset. b) $W_\lambda = f(P)$ curves of line satellites of Si II λ 6347 (filled circles) and Si II λ 6371 (open circles) of equivalent widths enhanced at phase 0.92 P. (Skulskij, 1993a).

the conditions for the excitation of different satellite lines shows the increase in temperature and the acceleration of the rotation of disk layers to the center of the gainer. However, the speed of their rotation is almost three times greater than the speed of the axial rotation of the gainer, which is approximately 85 km/s according to the simulations by Skulskij & Topilskaya (1991). This indicates certain autonomy of the satellite-disk rotation. Consequently, it should be adopted that the accretion disk consists of two parts around the hot disguised gainer: an external satellite-disk and an internal thick opaque disk, elongated also in the orbital plane.

It is important to note that the large axis of the satellite-disk is deflected in Fig. 1 outwards from the direction of motion of the gainer by about $(20-25)^\circ$. However, it was obvious, that in observations data, also taking into account the data of Struve (1941), Sahade (1966) and other researchers, there are fixed the long-period changes in the parameters of the satellite-disk. They were confirmed by Skulskij (1993b) as a result of a comprehensive study of changes in all spectral characteristics of the Si II $\lambda\lambda$ 6347, 6371 doublet, conducted separately for each of the seasons of Beta Lyrae observations in 1991-92. According to the result of observations 1992, the rotation of the elongated axis of the satellite disk was detected. For example, Fig. 4 shows the development of the spectral characteristics of satellite lines in the Si II $\lambda\lambda$ 6347, 6371 doublet from their appearance

to disappearance for the observations in 1991-92. There is a clear asymmetry in the radial velocity maxima at the 0.958 P and 0.022 P phases, which confirms the ellipsoidal shape of the satellite disk. But, the satellite lines in 1992 were clearly observed at the (0.009-0.014) P phases, whereas in 1991 they were visible only from the 0.021 P phase. In 1992, their equivalent widths increased sharply at phases of (0.920-0.925) P. Hence, the complex seasonal investigation of the absorption lines of both components and the emission in these Si II red lines showed a clear change in the conditions of the projection of the satellite-disk onto the surface of the bright donor due to the change in their relative configuration (Skulskij, 1993b). Over a year, the long axis of the satellite disk was deflected in the direction of the donor and turned counter-clockwise by about 45° . This result depicts rotation of the satellite-disk around the gainer, but it can also reflect precessional motion of this disk, in particular, with a period less than one year. In this regard, it should be noted that Osaki (1985) emphasized that the accretion disk can be deformed coherently into elliptical forms since they are the eigenmodes of such a disk.

3.4. Spectral observations of the Beta Lyrae system and masses its star components

Our spectral observations of the Beta Lyrae system began in the middle of the 1960s when there already was a substantive change of ideas about the evolution of binary systems. From the understanding of the new concept (Crawford, 1955), it followed that the hidden secondary component should be more massive, although underluminous for its mass. Therefore, investigating the complex spectrum of this binary system, apart from the obvious problems of the time, such as studying the chemical composition of the atmosphere of the bright component or elements of its orbit, the task was to find evidence of the line spectrum of the secondary component. From the articles of authoritative researchers of the Beta Lyrae system it followed that the absorption lines, which would track the motion of the secondary component in the spectrum of this binary system, are absent. However, Sahade (1966) observed that two absorption lines were visible in lines of the red doublet of silicon in addition to satellite lines. This spectral material was concentrated around the primary minimum, so these silicon lines were not sufficient for a different conclusion. That is why, during the discussion, on the question, what can explain the doubling of Si II absorption lines at certain phases, J. Sahade responds as follows: "One of the components gives velocities that agree with the lines of shell which surrounds the whole system, while the other arises from the primary (B8) star". Moreover, the absence of absorption lines of the secondary component in the Beta Lyrae spectrum was affirmed in a detailed review by Sahade (1980).

At this time, due to the importance of identifying the spectral lines of the secondary component (then the possibility of a black hole was also considered), a special time slot was allocated for the Beta Lyrae observations on the 2-m

telescope of the Shemakha Astrophysical Observatory. As a result, by Skulskij (1975b), the first determination of the masses of both components was carried out directly from the high-resolution spectrograms (0.1 Å/mm). Shallow and wide absorption lines of ionized elements, in particular, magnesium, the purple calcium doublet, and the red silicon doublet were detected, the radial velocities of which reflected the orbital motion of the secondary component at a mass ratio of approximately $q = 0.23$. The secondary component (currently the gainer) should be at least 4.3 times more massive than the bright donor.

More accurate determination of the orbital parameters of both components, determination of their masses and absolute dimensions of the Beta Lyrae system was carried out in the Si II $\lambda\lambda$ 6347, 6371 lines after a series of CCD observations on the 2.6-m CrAO telescope in 1989-1992 (see Skulskij & Topilskaya (1991) with the calculation of synthetic spectra) and Skulskij (1992, 1993b)). The mass ratio of the gainer to the donor reaches the value of 4.47 (with an error less than 0.1) and is of about $q = K_d/K_g = 0.224$ (here K_d and K_g are the semiamplitude of the radial velocities of the donor and the gainer, respectively). At an inclination of the orbit of about $i = 90^\circ$ and the mass of the donor in a range of (2.9 - 3.0) M_\odot , the mass of the gainer is in a range of (13 - 13.5) M_\odot . It is clear that the masses of both components need further consideration and a more precise definition for practical use.

First of all, one should take into account somewhat distorted profiles of the red silicon lines of both components due to variable and low ambient emission near these lines. Also, according to Skulskij (1993b), from the 1991 season to the 1992 season the off-season spectral differences in the lines of Si II $\lambda\lambda$ 6347, 6371 were recorded. In particular, this concerns significant changes in the equivalent widths of the absorption lines of both the donor and the gainer. The two-year averages for $K_d = 188.0$ km/s and for $K_g = 42.1$ km/s are within the 2 km/s between 1991 and 1992, with the maximum value in the 1992 season. Therefore, at least for the semiamplitude of the radial velocity of the donor, it is reasonable to prefer the less distorted lines of the donor atmosphere in the spectrum of the blue region. Our Beta Lyrae orbital elements obtained from observations on the 1.2-m CrAO telescope over 4 seasons in 1966-76 showed some differences, see Skulskij (1978). In particular, the average K_d values, determined from all measured lines of the blue region, are 185.2 km/s, varying within 0.4 km/s; but when determined only from the 5 Si II lines, they vary from 184.2 km/s in 1966 and 1969 to 186.8 km/s in 1972 and 1976, respectively.

An independent detailed analysis of our radial velocities, together with all published radial velocities over 100 years, was carried out thanks to a thorough investigation of Beta Lyrae orbital elements by Harmanec & Scholz (1993). The averaged value for K_d is (185.9 ± 0.33) km/s. There is also the averaged value K_g for all measurements of the gainer radial velocities up to 1992 inclusive: (41.4 ± 1.3) km/s. Then their determination of the component masses and the mass ratio is as follows: $M_g \sin^3 i = (12.94 \pm 0.05) M_\odot$, $M_d \sin^3 i = (2.88 \pm 0.10) M_\odot$ and $q = 0.223$. A similar analysis conducted by Ak et al. (2007) gives

$K_d = (185.27 \pm 0.20)$ km/s. The methodologically independent, first astrometric Beta Lyrae observations of Zhao et al. (2008), taking into account the spectral observations of other researchers, showed a somewhat smaller mass ratio $q = 0.222$ and masses of components of $M_d \sin^3 i = (2.83 \pm 0.18) M_\odot$ and $M_g \sin^3 i = (12.76 \pm 0.27) M_\odot$. Mourard et al. (2018), as well as in the recent modelings of the light curves from the far-ultraviolet to far-infrared regions, adopted the following values: $K_d = (186.30 \pm 0.35)$ km/s and $K_g = (41.4 \pm 1.3)$ km/s at $q = 0.222$.

Ultimately, the main purpose of such analysis is the need to optimize the masses of both components for further Beta Lyrae studies. Taking into account the previous analysis and all our observational data with some differences during this time, including 1992, the following values of $K_d = 186$ km/s and $K_g = 41.5$ km/s may be considered optimal, resulting in $q = 0.223$ and $M_g/M_d = 4.48$. Given the binary orbital inclination of $i = 92^\circ$ and $i = 93.5^\circ$, which were obtained respectively in Zhao et al. (2008) and Mourard et al. (2018), and, given all of the above, it is now possible to take as reliable the following values: $2.9 M_\odot$ for the donor and $13 M_\odot$ for the gainer. These masses of components are illustrated in Fig. 1. We used the donor mass of $2.9 M_\odot$ in Skulskyy et al. (2019) to calculate the inner structure of the donor, which precedes the formation of the degenerate dwarf. It was shown that the mass of such degenerate core of the donor should be in the range $(0.3-0.5) M_\odot$.

In view of the above, it is clear that the measurement of radial velocities had some difficulties due to the specificity of the physical conditions in the deformed donor atmosphere. The important role of the chemical composition of the donor atmosphere at the presence of such active mass losses should also be emphasized (Skulskij, 1975a). The donor absorption lines in the visible region belong mainly to the B8 III type star, but correspond to a broader excitation and ionization range and vary substantially with the orbital phase. The simultaneous presence of high excitation lines N II, C II, Si III, Fe III and a group of low excitation lines Fe I, Fe II, Ti II, Cr I, Cr II, and others is observed. A study of the dependence of chemical abundance on excitation conditions within the limits, which could exist in the donor atmosphere, has led to the conclusion that excess He, N, Si were obtained with all reasonable assumptions about the excitation conditions (Skulskij, 1986). The excess of He under the deficiency of H and the excess of N in comparison with C and O indicate that the atmosphere of the donor substance was significantly reworked during the combustion of hydrogen through the CNO cycle in the interior of the donor (this is consistent with the findings of Balachandran et al. (1986)). In addition, according to Skulskij (1975a, 1986), variations in the micro-turbulent velocities from 5.5 km/s in quadratures to 18 km/s on the side of the donor facing the gainer indicate the change in the atmospheric density along a deformed quasi-ellipsoidal surface of the donor at a practically filling of its Roche cavity. In this regard, it is interesting to note that the donor magnetic field was detected with its maximum on the side of the donor facing the gainer (Skulskij, 1985). In particular, the anomalous excess of

certain chemical elements on the donor surface is consistent with the magnetic Ap stars.

3.5. Spectral investigations and the magnetic field of the Beta Lyrae system

Magnetism as a phenomenon is widely studied in modern astrophysics. The basic question of how the magnetic field of stars originated and evolved remains unclear. It is more plausible that an anomalous chemical composition on the surface of stars is created during the evolution of stars (Romanyuk, 2005). The fraction of binary magnetic stars among CP-stars is insignificant, and the detailed study of their physical parameters and the identification of generation mechanisms and patterns in the behavior of their magnetic fields are limited by several objects (Skulsky & Romanyuk, 2009). From the point of view of stellar magnetism, the detection of magnetic field in the Beta Lyrae system was of particular interest. It is the only interacting binary system in which a magnetic rotator protrudes a giant of B-type that has reached its Roche cavity and is actively losing matter. The importance of this phenomenon requires an analysis of all known observations and investigations of the magnetic field.

The first consistent study of the Beta Lyrae magnetic field was carried out by Skulskij (1982, 1985, 1990) using four hundred Zeeman spectrograms with $9 \text{ \AA}/\text{mm}$ dispersion in the blue spectral region that were obtained over 31 nights in 1980-88 on the 6-m telescope of the Special Astrophysical Observatory (SAO). Zeeman splitting was measured in the atmospheric lines of the bright donor. These photographic observations have shown that the effective magnetic field strength varies quasi-sinusoidally over the orbital period, with the amplitude $A = (475 \pm 51) \text{ G}$ and the negative average value $H_e = (-1198 \pm 51) \text{ G}$. In order to elucidate the configuration of the magnetic field, Skulskij (1985) did the first model calculations. The agreement between the theoretical and the averaged observational phase curves for $H_e=f(P)$ was achieved as follows: a) the magnetic dipole axis is inclined to the orbit plane of the binary system by 28° ; b) the center of the magnetic dipole is displaced by $0.08 A$ from the donor center toward the gainer center (here A is the distance between centers of gravity of both components, see Fig. 1). In Burnashev & Skulskij (1991), based on the observations of all 31 nights in 1980-88, was refined that the axis of the donor magnetic dipole is directed along the meridian plane from phase $0.355P$ to phase $0.855P$ (see Fig. 5).

The spatial structure of the donor magnetic field and its change with the orbital period evoked some interest, but, first of all, all this required independent confirmation. There is an independent argument of the reality of the magnetic field, which is characteristic of magnetic stars: it is the depression at the $\lambda 5200 \text{ \AA}$ in their continuums. The phenomenon of depression at the $\lambda 5200 \text{ \AA}$ in the continuous spectrum of the Beta Lyrae system was detected and studied based on the absolute spectrophotometric data for 1974 and 1984 by Burnashev

& Skulskij (1986). They showed that the variability of the equivalent width of depression at 5200 Å clearly correlates during the orbital period with the variability of the magnetic field: both maxima of the equivalent width of this depression are observed at the same phases as the zones of both poles of the magnetic field on the donor surface.

The next were measurements of the Zeeman splitting of Si II $\lambda\lambda$ 6347, 6371 lines by Skulskij & Plachinda (1993). They were carried out in 1991-92 with a Stokesmeter and a CCD detector mounted on the 2.6-m CrAO telescope. These fairly homogeneous observations in all orbital phases are presented in Fig. 5 and 6 (as copies of Figures 1 and 2 from Skulskij & Plachinda (1993)).

The effective intensity of the longitudinal component of the magnetic field varies over an orbital period within ± 200 G, however, the shape of the curves and their amplitudes for each of the silicon lines are slightly different, although they somehow reflect the photographic curve of the magnetic field (of a mainly dipolar configuration). Fig. 6 shows, in particular, that changes in the magnetic field are clear only in the phases near the poles of the magnetic field, whereas in the phases near 0.5 P (the donor is in front of the observer) and in phases near 1.0 P (the donor is closed by the accretion disk) the magnetic field is almost zero. Moreover, the average magnetic field for 499 days of these CCD-observations is near -11 G. However, it can be seen from Fig. 5 and 6 that the polarity of the magnetic field clearly changes in the phases (0.32-0.39) P of the first quadrature and in the phases (0.82-0.89) P of the second quadrature. In both lines, these changes occur within 0.1 P, but in the central regions of the magnetic field poles, that is, exactly in the phases 0.355 P and 0.855 P, the field vanishes. The variability of the magnetic field occurs slightly differently at both poles, however, Fig. 5 and Fig. 6 show that the behavior of both magnetic field curves near the 0.855 P phases is similar (i.e., in the phases of observing the magnetic pole facing the gainer). Moreover, the behavior of the photographic curve of the magnetic field is also similar in the limits of these (0.81-0.88) P phases. This means that the physical conditions of the formation of the magnetic field along the transverse dimensions of this magnetic pole can differ substantially from both sides from the center of this pole.

Hence, the measurements of the Zeeman splitting of Si II $\lambda\lambda$ 6347, 6371 lines in Skulskij & Plachinda (1993) showed that magnetic field is formed on the donor surface mainly around the poles of the magnetic field, locally changing its polarity. These CCD observations allow the identification of both poles of the magnetic field on the donor surface. The transverse dimensions of both poles are given by the phase difference between the phases of change in the polarity of the magnetic field in both lines. The average of the phase difference is about 0.08 P. These observations independently confirm the presence of a hot region on the donor surface detected by the infrared photometry of Zeilik et al. (1982) in the phases (0.8-0.9) P (i.e., at the observation of the magnetic pole facing the gainer). This hot region was also detected by Skulskij (1993b) due to the deep eclipse of the region of the Si II emissions formation on the donor surface by the

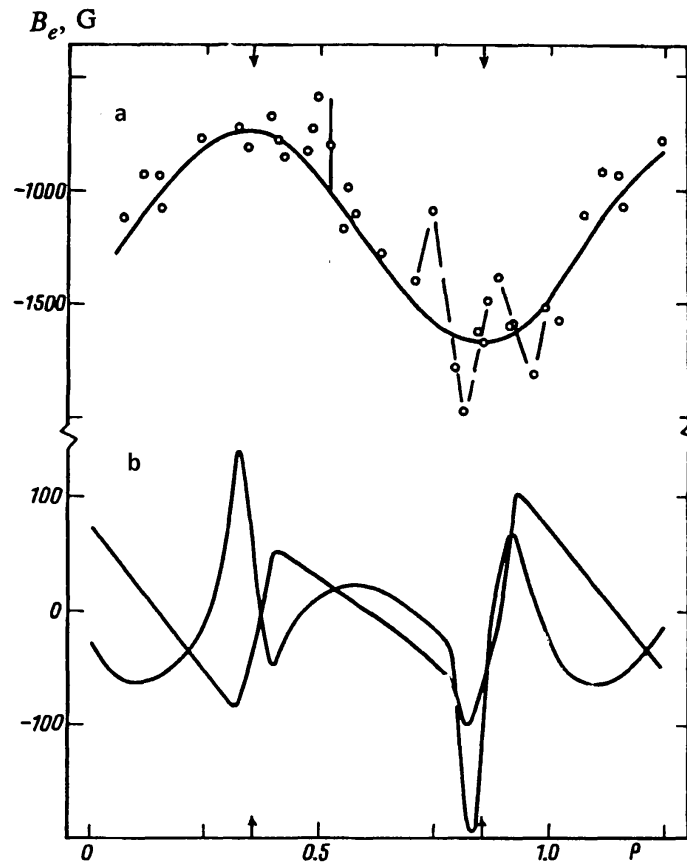


Figure 5. The photographic curve of effective magnetic-field strength plotted using data of Skulskij (1990). A characteristic error of measurements is shown by a vertical bar (2σ). The sinusoidal mean curve indicates the dipole field with poles at phases of 0.355 and 0.855 P (their centers are shown by arrows). In the region of visibility of the second pole, facing the massive gainer, rapid variations of the field are suspected (a). The averaged assumed $B_e=f(P)$ curves for both silicon lines from Figure 6 are given, in order to compare them with each other and with the photographic B_e -curve (see the text) (b).

satellite disk surrounding the gainer. It should be recalled that the Si II $\lambda\lambda$ 6347, 6371 absorption lines are limited by weak emission. The energy and dynamic characteristics of the absorption and the emission components of these lines show their variability, which is correlated synchronously with such variability of the donor magnetic field (Skulskij, 1993a,b). This study also has shown that both components of the Si II $\lambda\lambda$ 6347, 6371 lines are formed in a close spatial

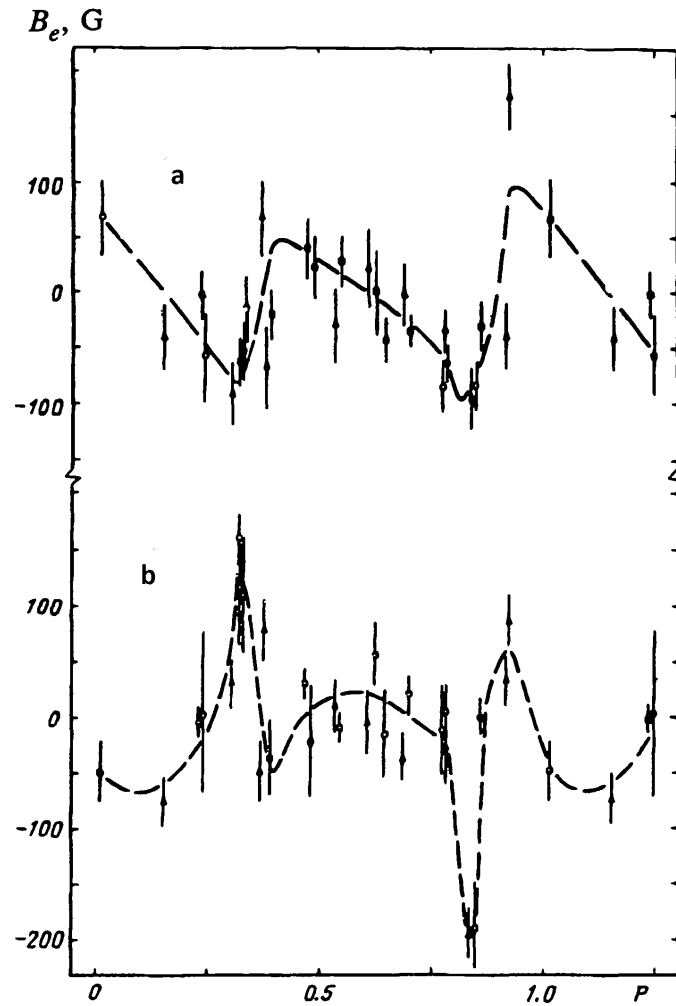


Figure 6. The phase variability of effective intensity of the longitudinal component of the magnetic field in Si II absorption lines λ 6347 (a) and λ 6171 (b) of the bright component, based on a study of Zeeman CCD spectrograms. Vertical error bars correspond to 2σ . Dashed curves were drawn by hand on the basis of assumed $B_e=f(P)$ variability.

environment near the donor atmosphere, which can reach the Roche cavity. Skulskij & Plachinda (1993) also noted that the magnetic field becomes less intense with the increasing height in the donor atmosphere.

In 1993-1995 and 2000-2004, CCD observations and Zeeman splitting mea-

measurements were continued, but in some metallic lines in the blue spectral region (Skulsky & Plachinda, 2005). Although these observations could not fully cover the orbital period, in general, the magnetic field demonstrated the time-dependent complicated behavior. For example, the arithmetic mean value of magnetic field for 20 observation dates 1993-1995 is (285.3 ± 95.5) G. In 1993-2004 five observation dates were obtained showing significant values of the magnetic field with the ratio $k = H_e/\sigma > (3-6)$ in the H_e ranges from -812 G to 1348 G. Special testing has shown that such magnetic field values are reliable. The possibility of the orbital and longer time-scale variability of the Beta Lyrae magnetic field is proposed in Leone et al. (2003) based on the dynamo mechanism. It should be noted that independent observations of the effective magnetic field, carried out over a 13-day full orbital period in June 1999 at the Osservatorio Astrofisico di Catania (OAcT), revealed magnetic field of positive polarity with an average value of (1.288 ± 163) kG. However, within the accuracy range, these measurements do not show any obvious changes in the magnetic field during the orbital period, and such OAcT observations were no longer repeated.

It should be noted that Skulskij & Plachinda (1993) also obtained the first data, that may indicate the presence of magnetic field in the pseudophotosphere of a thick accretion disk surrounding the gainer. It cannot be excluded that the magnetic field of the donor is in some way related to the magnetic field generated by the accretion disk, or that changes in the donor magnetic field may correspond to variations in the structures of the accretion disk. The frequency analysis of the magnetic field measurements did not reveal obvious periodic processes with long-term-scale variability, for example, with the well-known 283-day period. However, an agreed system of secondary periods and resonances was identified, which links the substructures of the accretion disk and the surface magnetized structures of the donor (Skulsky, 2007). The presence of a common magnetosphere, which can manifest itself in the circumstellar gas structures, cannot be excluded. Moreover, according to Shore & Brown (1990), in helium stars with a magnetically controlled matter (the atmosphere of the donor in the Beta Lyrae system also has excess helium), magnetized plasma can be directed outward from the magnetic polar regions on the star surface, forming the magnetosphere.

As it follows from the above analysis, all existing observations and measurements of the magnetic field, indicating its presence in the donor atmosphere, do not form the single magnetic field curve variability. This cannot rule out a long time magnetic field variability superimposed on the orbital period. Only two curves, the $H_e=f(P)$ as a photography curve in the blue region of spectrum (obtained from 1980-1988 observations on the 6-m SAO telescope) and such curve in the red region of spectrum (obtained from 1991-1992 CCD observations on the 2.6-m CrAO telescope in the silicon lines), show a certain correlation in the changes of the magnetic field over the orbital period. These CCD observations have shown that the magnetic field becomes apparent only at phases around the poles of the magnetic field obtained from the solution

of the photographic curve of the magnetic field. And the observations on the 6-m SAO telescope lead to an average value of the longitudinal magnetic field, that is significantly overestimated relative to such values in CCD observations. However, the quasi-sinusoidal photographic curve of the magnetic field looks as one would expect for magnetic stars. Thus, although the average magnetic field measured on the 6-m SAO telescope may be overestimated, such variability of the donor magnetic field should be considered important for further studies of the mass loss and accretion pattern in the Beta Lyrae system.

4. Short conclusion and outlook

The phase variability of the donor magnetic field and its specific configuration led to evident research of their interconnection with the configuration of the accretion gas structures in the Beta Lyrae system. This task remained relevant during long term observations and studies of the magnetic field. In the course of further processing of a large amount of research material, it became clear that there were a number of different observable facts that needed systemic coverage. This required a generalization of the current state of diverse, primarily spectral studies of the Beta Lyrae system. This idea worked. In the research conducted in this article, several important directions of work should be noted as of a definite basis for studying the processes of mass transfer in the presence of the magnetic field.

In order to optimize the mass of both components spectral and astrometric observations and model calculations of light curves were also analyzed. As a result, it can be argued that the currently optimal masses for the Beta Lyrae system are the following values: $2.9 M_{\odot}$ for the donor and $13 M_{\odot}$ for the gainer (they are illustrated in Fig. 1).

The study of satellite lines as a phenomenon in the Beta Lyrae spectrum led to the conclusion that the accretion disk consists of two parts: an outer satellite disk and an internal massive opaque disk, which have an ellipsoidal shape. The stratification of the excitation conditions of the various satellite lines shows an increase in the temperature and an acceleration of the rotation of the outer layers of the disk to the center of the gainer. A possible precessional movement of the accretion disk leads to its coherent deformation into elliptical forms as the eigenmodes of this disk. It turned out that the study of the spatial structure of the accretion disk and the secondary non-orbital periods of this binary system (e. g., the well-known 283-day period) should be carried out jointly taking into account the spatial configuration of the donor magnetic field. This led to forming a coherent system of secondary periods and resonances that change synchronously with the increase of the orbital period.

From the analysis of all observations and studies of the magnetic field, the long time variability of the magnetic field, in general, is still not clear. This phenomenon should be investigated more fully. It turned out that the systematic

observations of 1980-1988 on the 6-m SAO telescope could be considered as the most reliable data. They created a donor magnetic field curve over a long observation period similar to magnetic star curves. There is a spatial configuration of the donor magnetic field, based on model calculations, is suitable for further research of the question on the correlation between the orbital variability of the magnetic field and such variability of physical parameters in different processes, which take place between the components of the binary system. It is known that the structure of gas flows in the processes of accretion and mass exchange between the components of the binary system changes in a certain way over the orbital period. If these processes are reflected in the orbital variability of the magnetic field or vice versa, then it is necessary to consider their mutual influence and investigate them as a certain phenomenon.

The picture of the accretion of magnetized flows as a result of the preliminary study of the above correlation processes can be understood from Skulsky (2015, 2018). It has been found that the spatial configuration of the donor magnetic field influences the formation of magnetized gas structures between the components of the binary system. The collisions of the magnetized plasma with the accretion disk surrounding the gainer are especially effective in phases of the second quadrature when the heating of the accretion disk is greatly enhanced. This heating is also enhanced by the rapid counter-rotation of the accretion disk. The spatial configuration of the magnetic field of the donor is reflected by different physical processes in the accretion structures of this binary system. Further studies show this picture more fully, but this requires shedding light on a number of different observable facts from the far ultraviolet to the red region. Relevant materials are being prepared for coverage soon.

Acknowledgements. The author is thankful to S.I. Plachinda for constructive comments and V.I. Kudak for consultations.

References

- Ak, H., Chadima, P., Harmanec, P., et al., New findings supporting the presence of a thick disc and bipolar jets in the β Lyrae system. 2007, *Astron. Astrophys.*, **463**, 233, DOI: 10.1051/0004-6361:20065536
- Balachandran, S., Lambert, D. L., Tomkin, J., & Parthasarathy, M., The chemical compositions of algol systems - III. Beta Lyrae-nucleosynthesis revealed. 1986, *Mon. Not. R. Astron. Soc.*, **219**, 479, DOI: 10.1093/mnras/219.3.479
- Burnashev, V. I. & Skulskij, M. Y., Absolute spectrophotometry of beta Lyr. 1978, *Izv. Krymskoj Astrofiz. Obs.*, **58**, 64
- Burnashev, V. I. & Skulskij, M. Y., Short-period changes of H α emission in the β Lyrae. 1980, *Pisma v Astronomicheskii Zhurnal*, **6**, 587
- Burnashev, V. I. & Skulskij, M. Y., Variability of the 5200A Continuum Depression in Beta-Sagittarii and Nu-Sagittarii. 1986, *Sov. Astron. Lett.*, **12**, 225

- Burnashev, V. I. & Skulskij, M. Y., H α photometry and the magnetic field of β Lyrae. 1991, *Izv. Krymskoj Astrofiz. Obs.*, **83**, 108
- Crawford, J. A., On the Subgiant Components of Eclipsing Binary Systems. 1955, *Astrophys. J.*, **121**, 71, DOI: 10.1086/145965
- Goodricke, J. & Englefield, H. C., Observations of a New Variable Star. By John Goodricke, Esq.; Communicated by Sir H. C. Englefield, Bart. F. R. S. and A. S. 1785, *Philosophical Transactions of the Royal Society of London Series I*, **75**, 153
- Harmanec, P., Morand, F., Bonneau, D., et al., Jet-like structures in β Lyrae. Results of optical interferometry, spectroscopy and photometry. 1996, *Astron. Astrophys.*, **312**, 879
- Harmanec, P. & Scholz, G., Orbital elements of beta Lyrae after the first 100 years of investigation. 1993, *Astron. Astrophys.*, **279**, 131
- Ignace, R., Oskinova, L. M., Waldron, W. L., Hoffman, J. L., & Hamann, W. R., Phase-dependent X-ray observations of the β Lyrae system. No eclipse in the soft band. 2008, *Astron. Astrophys.*, **477**, L37, DOI: 10.1051/0004-6361:20078871
- Kondo, Y., McCluskey, G. E., Silvis, J. M. S., et al., Ultraviolet Light Curves of beta Lyrae: Comparison of OAO A-2, IUE, and Voyager Observations. 1994, *Astrophys. J.*, **421**, 787, DOI: 10.1086/173691
- Leone, F., Plachinda, S. I., Umana, G., Trigilio, C., & Skulsky, M., The magnetic field of the β Lyrae system: Orbital and longer time-scale variability. 2003, *Astron. Astrophys.*, **405**, 223, DOI: 10.1051/0004-6361:20030550
- Mennickent, R. E. & Djurašević, G., On the accretion disc and evolutionary stage of β Lyrae. 2013, *Mon. Not. R. Astron. Soc.*, **432**, 799, DOI: 10.1093/mnras/stt515
- Mourard, D., Brož, M., Nemravová, J. A., et al., Physical properties of β Lyrae A and its opaque accretion disk. 2018, *Astron. Astrophys.*, **618**, A112, DOI: 10.1051/0004-6361/201832952
- Osaki, Y., Irradiation-induced mass-overflow instability as a possible cause of super-outbursts in SU UMa stars. 1985, *Astron. Astrophys.*, **144**, 369
- Peel, M., The 340-d period in beta Lyrae. 1997, *Mon. Not. R. Astron. Soc.*, **284**, 148, DOI: 10.1093/mnras/284.1.148
- Romanyuk, I. I., Magnetic CP stars of the main sequence. I. Diagnostic techniques for magnetic field. 2005, *Bulletin of the Special Astrophysics Observatory*, **58**, 64
- Sahade, J., On the System of β Lyrae. 1966, *IAU Trans.*, **12B**, 494
- Sahade, J., The system of β Lyrae. 1980, *Space Sci. Rev.*, **26**, 349, DOI: 10.1007/BF00217387
- Shore, S. N. & Brown, D. N., Magnetically Controlled Circumstellar Matter in the Helium-strong Stars. 1990, *Astrophys. J.*, **365**, 665, DOI: 10.1086/169520
- Skulskij, M. Y., Quantitative analysis of the beta Lyrae spectrum: study of the atmosphere of the bright component. 1975a, *Probl. Cosm. Phys., Bull. Kiev Univer., Astron. Ser.*, **10**, 160

- Skulskij, M. Y., Quantitative analysis of the spectrum of Beta Lyrae IV. Identification of lines of weak component and masses of stars in close binary. 1975b, *Astron. Zh.*, **52**, 710
- Skulskij, M. Y., Orbital elements of β Lyrae (observations in the spring of 1976). 1978, *Tsirk. Lviv Astron. Obs.*, **53**, 7
- Skulskij, M. Y., Beta Lyrae as a magnetic binary star. 1982, *Sov. Astron. Lett.*, **8**, 126
- Skulskij, M. Y., The Magnetic Field of the Beta-Lyrae System. 1985, *Sov. Astron. Lett.*, **11**, 21
- Skulskij, M. Y. 1986, Astrophysics and Space Science Library, Vol. **125**, *β Lyrae - a Binary System with Anomalous Abundances and Magnetic Field*, ed. C. R. Cowley, M. M. Dworetzky, & C. Megessier (Springer Netherlands), 365
- Skulskij, M. Y., The magnetic field and tidal resonant phenomena in of β Lyrae. 1990, *Mitteilungen KSO Tautenberg*, **125**, 146
- Skulskij, M. Y., Study of β Lyrae CCD spectra. Absorbtion lines, orbital elements and disk structure of the gainer. 1992, *Sov. Astron. Lett.*, **18**, 287
- Skulskij, M. Y., Study of Beta Lyrae CCD spectra - Characteristics of the SiII $\lambda\lambda$ 6347, 6371 doublet and the discovery of the cyclic variability of equivalent widths of lines of the loser's 'magnetized' atmosphere. 1993a, *Astronomy Letters*, **19**, 19
- Skulskij, M. Y., Study of beta Lyrae spectrum. Characteristics of SiII $\lambda\lambda$ 6347, 6371 doublet in 1992 and their variability from season to season. 1993b, *Astronomy Letters*, **19**, 160
- Skulskij, M. Y., Study of the β Lyrae spectrum. Matter transfer and circumstellar structures in presence of the loser's magnetic field. 1993c, *Astronomy Letters*, **19**, 45
- Skulskij, M. Y. & Plachinda, S. I., A study of the magnetic field of the bright component of β Lyr in the SiII $\lambda\lambda$ 6347, 6371 lines. 1993, *Astronomy Letters*, **19**, 203
- Skulskij, M. Y. & Topilskaya, G. P., Secondary Component Lines in the Spectrum of Beta-Lyrae. 1991, *Sov. Astron. Lett.*, **17**, 263
- Skulsky, M. Y., Magnetic rotator and its evidence in β Lyrae system. 2000, *Kinematika i Fizika Nebesnykh Tel Supplement*, **3**, 425
- Skulsky, M. Y., Magnetic fields and secondary rhythms in the Beta Lyrae system. 2007, in *Physics of Magnetic Stars*, ed. I. I. Romanyuk, D. O. Kudryavtsev, O. M. Neizvestnaya, & V. M. Shapoval, 223–229
- Skulsky, M. Y., On the nature of the interacting β Lyrae system: location of hot region on accretion disk as representation of the magnetized gas structures. 2015, *Science and Education a New Dimension. Natural and Technical Sciences*, **III**, 6
- Skulsky, M. Y., On the structure of magnetized accretion flows in the system of Beta Lyrae. 2018, *Contrib. Astron. Obs. Skalnaté Pleso*, **48**, 300
- Skulsky, M. Y. & Plachinda, S. I., The magnetic field of β Lyrae. 2005, in IAU Symposium, Vol. **224**, *The A-Star Puzzle*, ed. J. Zverko, J. Ziznovsky, S. J. Adelman, & W. W. Weiss, 647–651

- Skulsky, M. Y. & Romanyuk, I. I., β Lyrae and magnetic field of binary stars. 2009, *Izv. Krymskoj Astrofiz. Obs.*, **104**, 68
- Skulskyy, M. Y., Vavrukh, M. V., & Smerechynskiy, S. V., X-ray binary Beta Lyrae and its donor component structure. 2019, *Proceedings of the International Astronomical Union*, **14**, 139142, DOI: 10.1017/S174392131900111X
- Struve, O., The Spectrum of β Lyrae. 1941, *Astrophys. J.*, **93**, 104, DOI: 10.1086/144249
- Umana, G., Maxted, P. F. L., Triguero, C., et al., Resolving the radio nebula around beta Lyrae. 2000, *Astron. Astrophys.*, **358**, 229
- Van Hamme, W., Wilson, R. E., & Guinan, E. F., Periodic Light Curve Changes for Beta Lyrae. 1995, *Astron. J.*, **110**, 1350, DOI: 10.1086/117609
- Zeilik, M., Heckert, P., Henson, G., & Smith, P., Infrared photometry of beta Lyrae: 1977-1982. 1982, *Astron. J.*, **87**, 1304, DOI: 10.1086/113217
- Zhao, M., Gies, D., Monnier, J. D., et al., First Resolved Images of the Eclipsing and Interacting Binary β Lyrae. 2008, *Astrophys. J., Lett.*, **684**, L95, DOI: 10.1086/592146

Note on magnitude estimation on digitized astronomical photographic plates

R. Hudec^{1,3} and E. Splittgerber²

¹ *Czech Technical University in Prague, Faculty of Electrical Engineering,
Prague, Czech Republic, (E-mail: hudecren@fel.cvut.cz)*

² *Sonneberg Observatory, Sonneberg, Germany*

³ *Kazan Federal University, Kazan, Russian Federation*

Received: June 10, 2020; Accepted: June 30, 2020

Abstract. The scanned astronomical archival plates offer the possibility of alternative analyses on these data. Apart from a complete evaluation by sophisticated computer programs, the recent efforts offer an alternative fast method of eye estimation method using scanned plates exhibited on computer screens. This alternative method has been investigated by analyzing the light curve of XX Cep on several hundred scanned sky patrol plates from the Sonneberg Observatory plate archive.

Key words: sky surveys – astronomical photography – astronomical plate digitization

1. Introduction

There are about 10 million astronomical photographic glass plates and negatives in the plate archives over the globe (Hudec, 2019, 2014, 2007). A large fraction of them were taken for purposes of variable star research. The methods applied in the past to approach and analyze these data included plate photometry by dedicated plate photometers (e.g. iris photometers) as well as eye estimate methods, and more recently the computer analyses based on scanned data. The method of eye estimates, based on the original Argelander method or similar alternative methods, was widely used over the past 100 years in variable star research and has resulted in numerous scientific publications until recently, e.g. (Hudec et al., 2013). Over many decades, it was the mostly used method to access the data recorded in astronomical archival plates and to yield the variable star magnitudes. At many centers of variable star research, such as the Sonneberg Observatory in Germany (Hudec, 2007; Kroll, 2009), it represented the mostly used method (Hudec, 1999). The obvious preference of this method was that it was fast (in contrast to plate photometers which were slow), on the other side it has required some non-trivial skills and hence only experienced observers were able to achieve a reasonable accuracy of the measurements. However, an experienced observer was able to provide accuracy of measurements analogous

to or even in some cases exceeding those obtained with plate photometers, see e.g. (Hudec & Wenzel, 1976).

Recently, many observatories with plate collections have started (partly extended) scanning efforts, both with dedicated custom-made plate scanners as well as with commercial flatbed scanners. One of the most extended scanning was at the Sonneberg Observatory, Germany, where the largest European astronomical plate archive with about 280 000 plates is deposited. So far 237 430 plates have been scanned there. The data were stored on DVDs and hard discs (Kroll, 2009)¹.

In addition to that, there are two major scanning projects with automated pipelines to access and evaluate digitized plate data:

(i) APPLAUSE (Germany Hamburg, Bamberg, Potsdam) 70 276 plates so far², (Tuvikene et al., 2014) and (ii) DASCH Harvard College Observatory (HCO) USA 395 921 plates so far (Grindlay et al., 2012)³.

As a consequence of converting the information recorded on astronomical sky plates, novel methods of data mining and data analyses have appeared (Hudec, 2019; Hudec & Hudec, 2014). While the most important one rely on evaluation of the digitized data by powerful computers and dedicated software programs, there is another interesting alternative as described in this contribution, and this is the eye estimate on a computer screen instead of with a microscope and original plates.

The obvious preference of this method is that it is fast (as in the case of estimates on original plates) but the additional preference is that this work can be done remotely also without approaching the plates.

2. XX Cep as a test object

As it was not very clear what the accuracy in this case will be, we have performed a test study. We have selected a variable eclipsing binary XX Cep as the test object. XX Cephei (HD 222217) was discovered photographically by Schneller (1928). Interest in this partially eclipsing Algol system centered on the systems possible apsidal motion. The evidence for apsidal motion was based on the eccentric spectroscopic orbit determined by Struve (1946), a displaced secondary minimum reported by Iljasova (1946), Fresa (1956), and Lavrov (1957), and possible cyclic changes in the period, see Mayer (1984). Mardirossian et al. (1980) obtained a photometric solution from a reanalysis of the Fresas data. The most recent photometric solution was by Bonifazi & Guarnieri (1986) based on observations made with the 60 cm telescope at Bologna Observatory.

¹<https://www.plate-archive.org/applause/wp-content/uploads/2019/04/Kroll.PhotographicAndDigitalSkySurveysAtSonnebergObservatory.pdf>

²<https://www.plate-archive.org/applause/>

³<http://dasch.rc.fas.harvard.edu/lightcurve.php>

XX Cephei is a system with a changing period, probable mass exchange, and a possible light-time effect from a third stellar companion. It was shown that a continuous period change coupled with a light-time effect is a plausible explanation for the period changes (Angione & Sievers, 2006). A spectroscopic search for evidence of mass transfer and features of the cooler component yielded no positive results (Angione & Sievers, 2006).

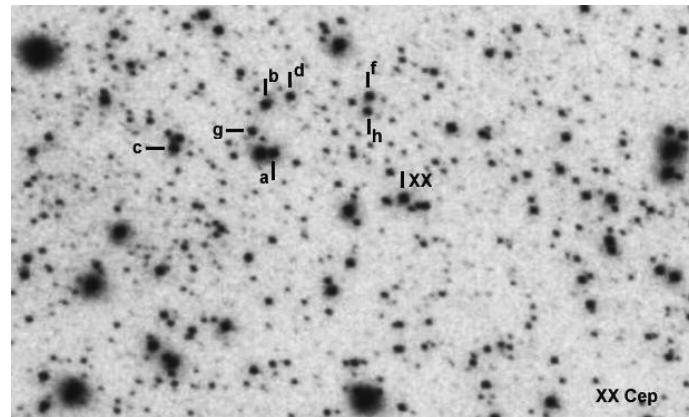


Figure 1. The area of XX Cep on the scanned Sonneberg sky patrol plate with the variable star indicated, as well as comparison stars used for the measurements.

The star was measured by one of us (ES) on 950 blue sensitive sky patrol plates taken between 1958 and 1995 by the patrol cameras at the Sonneberg Observatory. For the study, the original scanned data were unzipped and then transferred from a tiff format to a jpeg image format with following visualization on a laptop screen (Fig. 1). Then the eye estimation method was applied in a similar manner as usual. We note that the star was about 4 magnitudes brighter than the limiting magnitude on the negatives used. Typically, stars of this magnitude have the best accuracy in case of eye estimates. The resulting orbital light curve of the test variable star is shown in Fig. 2. The elements from the literature (Bonifazi & Guarnieri, 1986) have been used to construct this curve. It is obvious that the mean measurement error in this case amounts to about 0.1 mag, which is a typical value for an eye estimation method of this type of plate material.

3. Discussion

The amateur astronomers have always provided a valuable contribution to data analyses recorded on astronomical archival plates. They were regular visitors to many observatories with large plate collections. Nowadays, after the relevant

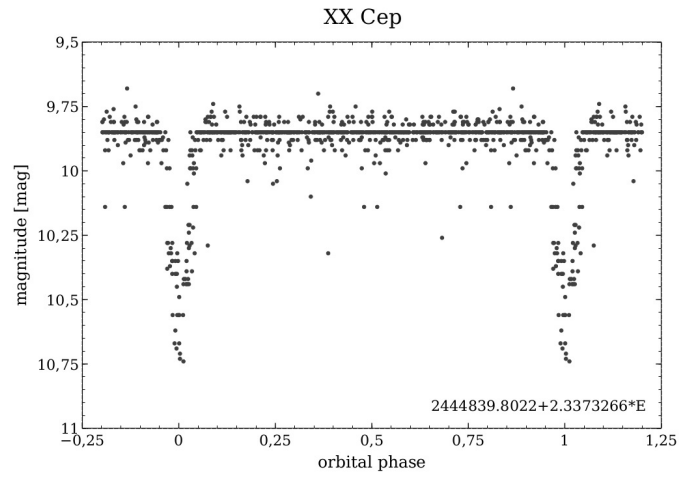


Figure 2. The orbital light curve of XX Cep generated by the method described and discussed in this paper.

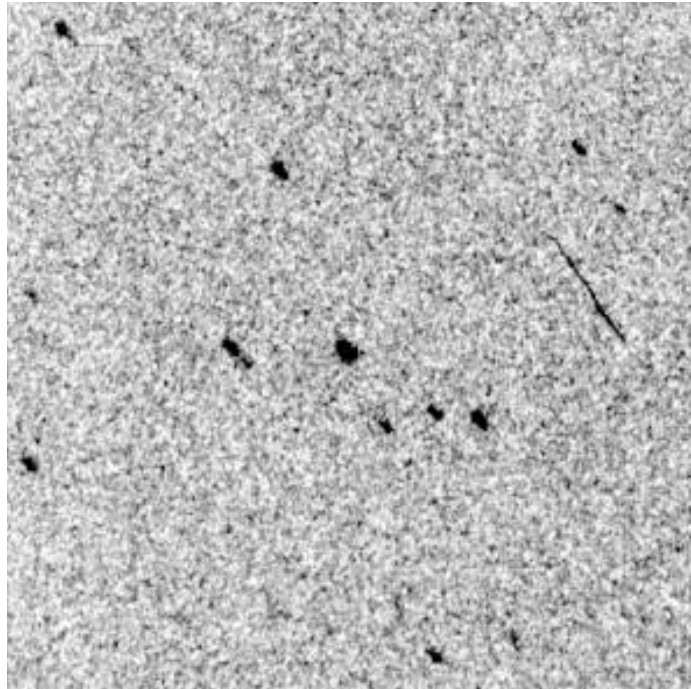


Figure 3. The area of XX Cep on the scanned HCO plate, the target is in the center.

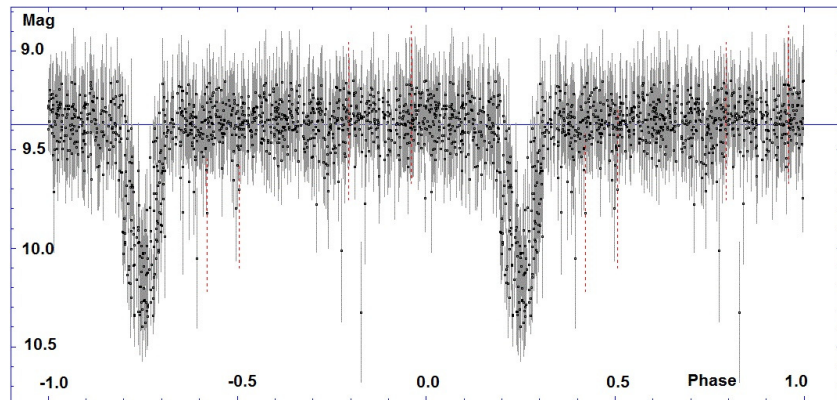


Figure 4. The orbital light curve of XX Cep generated by the automated DASH pipeline.

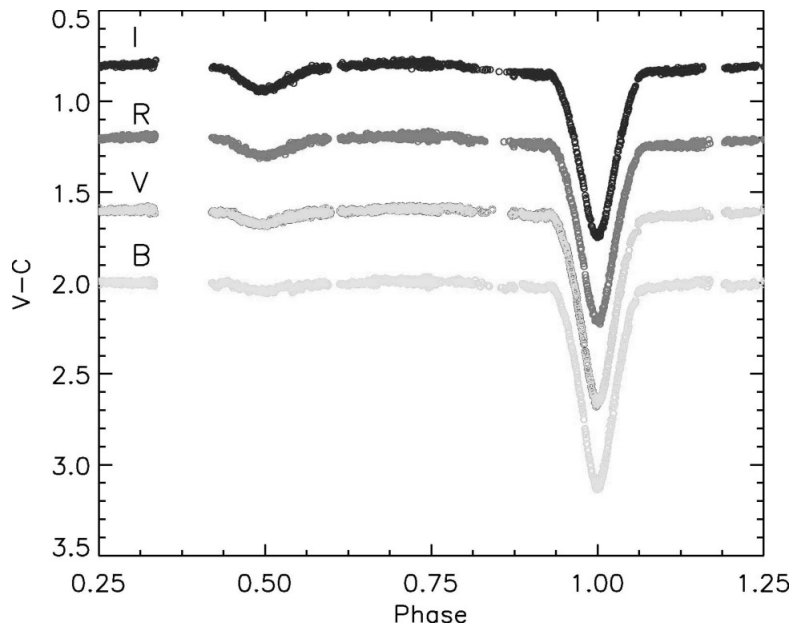


Figure 5. The orbital light curve of XX Cep based on CCD observations by 40 cm and 35 cm telescopes (for comparison) (Hosseinzadeh et al., 2014). It shows that the small secondary minimum around phase 0.5 is almost invisible in the B filter (note that the Sonneberg photographic data used in our study are blue sensitive, i.e. close to it).

plates were fully scanned, they have an alternative possibility, namely to analyze the digitized plates remotely on their laptops. While the emphasis of plate analyses must rely on a sophisticated evaluation of scanned data by computers and dedicated software packages, at the same times the eye estimates can contribute to some special related aspects.

For a comparison, we have created an analogous light curve of XX Cep using the automated DASCH pipeline analyzing scanned HCO plates. (Figs. 3 and 4). It is evident that the scatter in the generated light curve exceeds the scatter of the light curve obtained by our method described in this paper. The small secondary minimum in the orbital light curve of XX Cep visible in data sets provided by photoelectric photometry and CCD telescopes is invisible in our orbital light curve (Fig. 2) but we note that, albeit the photographic observations are always limited in their accuracy covering small details less than 0.1 mag, the amplitude of secondary minima depends on wavelength, being less prominent in the blue band (Fig. 5).

4. Conclusions

We conclude that the accuracy of the eye estimation method performed with digitized plate data visualized on a computer (laptop) screen is similar to that obtained for direct eye estimates on original plates with the use of a microscope.

Acknowledgements. The authors are extremely thankful to the staff of the Sonneberg Observatory. This work was partly supported by GACR grant 13-33324S and by the MSMT Mobility project 8J18AT036. We thank the referee, Dr. Sergei Shugarov, for his valuable comments improving the paper.

References

- Angione, R. J. & Sievers, J. R., The Algol System XX Cephei. 2006, *Astron. J.*, **131**, 2209, DOI: 10.1086/501009
- Bonifazi, A. & Guarnieri, A., Photoelectric study of the low-mass semidetached system XX Cephei. 1986, *Astron. Astrophys.*, **156**, 38
- Fresa, A., Curva di luce fotoelettrica ed orbita della variabile ad eclisse X X Cephei. 1956, *Memorie della Societ Astronomia Italiana*, **27**, 299
- Grindlay, J., Tang, S., Los, E., & Servillat, M., Opening the 100-Year Window for Time-Domain Astronomy. 2012, in IAU Symposium, Vol. **285**, *New Horizons in Time Domain Astronomy*, ed. E. Griffin, R. Hanisch, & R. Seaman, 29–34
- Hosseinzadeh, B., Pazhouhesh, R., & Yakut, K., Observations, light curves analysis and pulsation behavior of the Algol-type eclipsing binary system XX Cep. 2014, *New Astronomy*, **27**, 95, DOI: 10.1016/j.newast.2013.08.005
- Hudec, R., An introduction to the world's large plate archives. 1999, *Acta Historica Astronomiae*, **6**, 28

- Hudec, R. 2007, *Astrophysics with Astronomical Plate Archives*, ed. A. P. Lobanov, J. A. Zensus, C. Cesarsky, & P. J. Diamond, 79
- Hudec, R., Digitized Astronomical Photographic Archives as Large Area Sky Survey of Large Amount of Astronomical Data. 2014, in *Proceedings of Frontier Research in Astrophysics (FRAPWS2014) held 26-31 May, 2014 in Mondello (Palermo), Italy*. Online at <https://pos.sissa.it/237/039/pdf>, 39
- Hudec, R., Astronomical photographic data archives: Recent status. 2019, *Astronomische Nachrichten*, **340**, 690, DOI: 10.1002/asna.201913676
- Hudec, R., Bašta, M., Pihajoki, P., & Valtonen, M., The historical 1900 and 1913 outbursts of the binary blazar candidate OJ287. 2013, *Astron. Astrophys.*, **559**, A20, DOI: 10.1051/0004-6361/201219323
- Hudec, R. & Hudec, L., US Astronomical Photographic Data Archives: Hidden Treasures and Importance for High-Energy Astrophysics. 2014, in *Multifrequency Behaviour of High Energy Cosmic Sources*, 316–319
- Hudec, R. & Wenzel, W., Observations of HZ Her/Her X-1 on Sonneberg Astrograph Plates. 1976, *Bulletin of the Astronomical Institutes of Czechoslovakia*, **27**, 325
- Iļjasova, N., XX Cephei. 1946, *Engelhardt Astron. Obs. Bull.*, **24**, 12
- Kroll, P., Real and Virtual Heritage - The Plate Archive of Sonneberg Observatory - Digitisation, Preservation and Scientific Programme. 2009, in *Cultural Heritage of Astronomical Observatories: From Classical Astronomy to Modern Astrophysics*, ed. G. Wolfschmidt, 311–315
- Lavrov, M. I., The Eclipsing Variable Star XX Cephei. 1957, *Peremennye Zvezdy*, **12**, 21
- Mardirossian, F., Mezzetti, M., Cester, B., Giuricin, G., & Russo, G., Revised photometric elements of five possible sd-d systems. 1980, *Astron. Astrophys., Suppl.*, **39**, 235
- Mayer, P., Periodic Terms in the Light Elements of XX CEP and RW Per. 1984, *Bulletin of the Astronomical Institutes of Czechoslovakia*, **35**, 180
- Schneller, H., Das System RS Canum venaticorum. 1928, *Astronomische Nachrichten*, **233**, 361, DOI: 10.1002/asna.19282332202
- Struve, O., Spectrographic Observations of Eleven Eclipsing Binaries. 1946, *Astrophys. J.*, **103**, 76, DOI: 10.1086/144790
- Tuvikene, T., Edelmann, H., Groote, D., & Enke, H., Work flow for plate digitization, data extraction and publication. 2014, in *Astroplate 2014*, 127

PRÁCE ASTRONOMICKÉHO OBSERVATÓRIA
NA SKALNATOM PLESE
L, číslo 3

Zostavovateľ:	RNDr. Richard Komžík, CSc.
Vedecký redaktor:	RNDr. Augustín Skopal, DrSc.
Vydal:	Astronomický ústav SAV, Tatranská Lomnica
IČO vydavateľa:	00 166 529
Periodicita:	3-krát ročne
ISSN (on-line verzia):	1336-0337
CODEN:	CAOPF8
Rok vydania:	2020
Počet strán:	70

Contributions of the Astronomical Observatory Skalnaté Pleso are processed using
 $\LaTeX 2_{\epsilon}$ CAOSP DocumentClass file 3.07 ver. 2019.